ABSTRACT

ORTON, NIGEL PAUL. Boundary Layer Energy Transport in Plasma Devices. (Under the direction of John G. Gilligan and Mohamed A. Bourham.)

The purpose of this research was to develop a model of boundary-layer energy transport in electric launchers, and perform a numerical simulation to investigate the influence of turbulence, thermal radiation and ablation on energy flux to plasma-facing surfaces. The model combines boundary-layer conservation equations with a k-ω turbulence model and multi-group radiation transport, and uses plasma models for fluid properties such as viscosity, thermal conductivity and specific heat capacity. The resulting TURBFIRE computer code is the most comprehensive simulation to date of boundary-layer turbulence and radiation transport in electric launcher plasmas.

TURBFIRE was run for cases with and without ablation. Temperature and velocity profiles are presented for all code runs, as are values of heat flux to the wall. The results indicate that both radiation transport and turbulence are important mechanisms of energy transport in the boundary layer, and therefore that both should be modeled in future simulations. Additionally, heat flux to the wall via both conduction and radiation was found to be significant for all cases run. Other authors have theorized that conduction could be neglected, but the current results show that this is not the case near the wall.

This research is also novel for its advances in computational fluid dynamics (CFD). The energy equation was written in terms of internal energy and discretized in a manner more implicit than in typical CFD codes. These changes were necessary to enable the code to accurately calculate heat capacity, which changes greatly with temperature for even weakly-ionized plasmas. Additionally, zero-gradient boundary conditions were used at the free stream for the turbulent kinetic energy and its dissipation rate (k and ω). Experimentally determined values of k_{fs} and ω_{fs} are typically used in CFD codes, but these data are not available for most plasma devices.

BOUNDARY LAYER ENERGY TRANSPORT IN PLASMA DEVICES

by

NIGEL PAUL ORTON

A dissertation submitted to the Graduate Faculty of
North Carolina State University
in partial fulfillment of
the requirements for the Degree of
Doctor of Philosophy

Department of Nuclear Engineering

Raleigh

2000

Approved By:

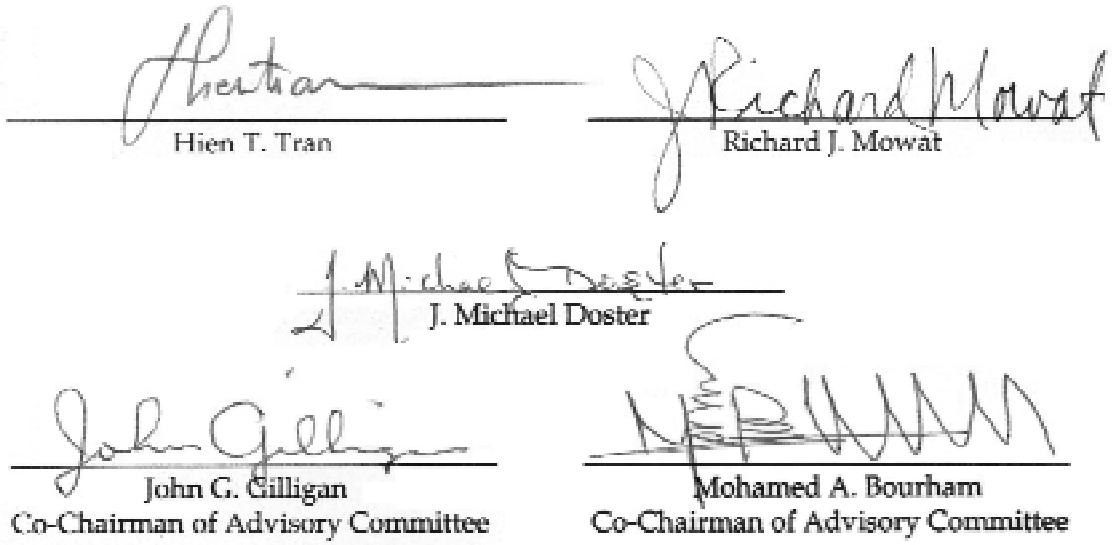

"We shall not cease from explorations
And the end of all our exploring
Will be to arrive where we started
And know the place for the first time."

-- T. S. Eliot, *Four Quartets*

"*Spend* the afternoon. You can't take it with you."

--Annie Dillard, *A Pilgrim at Tinker Creek*

BIOGRAPHY

Sitting on the beach south of Fort Fisher NC, getting sandblasted by 30 MPH winds, I contemplate my two-page autobiography. From what I can tell, the graduate school intends for me to spit out a few dry facts. If you haven't already turned the page I guess you deserve to know a little more than just that.

I like music, mountains and books. One of my favorite authors is Edward Abbey. He wouldn't pass up the opportunity to throw in a few sentences about jellyfish, and sand in your hair and your eyes and your sandwich, and how you'd be much happier if you just stayed at home. Then he'd ruin everything by telling you about the spray blowing from the tops of the waves and the seagull surfing the wind hoping for a scrap of his lunch, and he'd stumble into a story that would leave you no choice but to come and see it all for yourself. As for me, having just suffered my first Wisconsin winter I'd be out here on the beach writing even if it were pouring with rain. You can be sure I'd enjoy it, too.

I was born in Ilford, Essex, England on December 21st, 1965, but I don't remember much about the place since we caught a boat to the US that summer. Dad says my mom was green as a lime the whole way. I was soon joined in the world by Susanne and Philip, who managed to thrive despite their hyperactive older brother. Denville, NJ and Warwick, RI were ideal places for a kid to grow up. We had 2½ feet of snow once in Rhode Island. The sledding was the best ever!

When I was fifteen we moved to Grosse Pointe, MI, where I graduated from high school in 1983.

I earned my B.S. in nuclear engineering from the University of Michigan, and soon afterwards moved to North Carolina to attend NC State. Despite the rigors of academia, I took advantage of my time here to further my education in fields beyond the usual scope of nuclear engineering. Schoolbooks and classes are fascinating, but a physicist ought to have an understanding of the world far beyond what a classroom education can provide.

In 1994, I met Olga Lucia Herrera in a convenience store outside of Atlanta. We chatted over a few margaritas, then went to her motel room. I slept on the floor (as did the friends who were with us), and the next morning we set off on the camping trip we had arranged with our mutual friend Mark. Thanks Mark! (and sorry I stood you up for lunch today.) Olga Lucia and I were married on January 9th, 1999 in her hometown of Popayán, Colombia. In June of that year we moved to Madison, WI, where I began a residency in medical physics at the University of Wisconsin Hospital. Thus far we have thoroughly enjoyed both Madison and our new jobs.

ACKNOWLEDGEMENTS

I would first like to express my sincere appreciation to my parents, Colin and Barbara, for their love, patience and unwavering support. Without any one of these the completion of this project would not have been possible. I would also like to thank my wife, Olga Lucia, for her encouragement and ability to be in a good mood whenever mine is bad, and all of my friends and professors for their aid, encouragement, friendship, support and perspective, whether within or outside of the university. I hope many of our friendships will carry on into the future.

Special thanks go to my professors John Gilligan, Mohammed Bourham, Mike Doster and Kuruvilla Verghese, for their support, guidance and patience; to my closest friends at NCSU, Roma Mohanti, Rifat Alchalabi, Sai Tallavarjula and Jorge Duarte, for their friendship and good nature during the hardest times of our common plight; to Nick Speaks, bj bowen and Martha Mikkelson for many late-night conversations that helped me to maintain a healthy perspective on life in graduate school; to Emma Garnett and “Doc. B” Satterfield for treating Olga Lucia and me like family, and for doing so much to help make the past few months bearable; to Cathy Richards for her great cooking and perpetual good nature, and for tea sweet enough to crystallize your teeth; to my friends from the NCSU Forestry, Soil Science and Physical Education departments, for accompanying me on explorations of the North Carolina mountains and beaches, and for sharing their knowledge and insight which made our trips much richer; and finally to Dr. Ray

Porter and Felipe Herrera, who I thought would be around to share in today's celebration. I will always miss Dr. Porter's enthusiasm and Felipe's welcome knocks on the door around dinnertime.

TABLE OF CONTENTS

LIST OF TABLES

LIST OF FIGURES

NOTATION

Quantities with the symbol $^-$ are time-averaged. Those with the symbol $^\sim$ are mass-weighted means.

C_V	specific heat at constant volume
C_P	specific heat at constant pressure
c	speed of light in a vacuum
E_R^g	energy density for radiation in group g
E_{RP}^g	equilibrium energy density for radiation in group g
f_{abl}	fraction of incident energy that goes into ablation
f_{tr}	energy transmission fraction
g_I	degeneracy of ionization state i
H_{sub}	heat of sublimation
h	Planck constant
k	turbulent kinetic energy
k_B	Boltzmann constant
k_{th}	thermal conductivity
K_R^g	radiation conductivity for grp g
l	scale length for turbulence
m_e	electron rest mass
n	number density
P	pressure
Pr_T	turbulent Prandtl number
$\overline{Q}_{en}$	momentum-transfer cross-section for e^--neutral collisions
q"	heat flux incident on the surface
R	gas constant
T	temperature
U	internal energy
u^+	dimensionless velocity ($= v_{x,fs} / u_\tau$)
u_τ	friction velocity
v_x	velocity parallel to the surface
v_y	velocity normal to the surface
v_{th}	thermal velocity
x	direction parallel to the surface
y	direction parallel to the surface
y^+	dimensionless distance ($=u_\tau y / \nu$)
$\bar{z}$	average ionization
Z	average ionic charge

Greek Letters:

α, β^*	empirical constants in the k-ω equations
ε	turbulent KE dissipation rate
ε_0	permittivity of free space
Λ_m	modified Coulomb parameter
λ	mean free path
μ	viscosity
μ_T	eddy viscosity
ν_{eH}	collision frequency for electron-heavy particle collisions
ν_{ei}	collision frequency for electron-ion collisions
ρ	mass density
σ	Stefan-Boltzmann constant
σ_k	turbulent Prandtl-Schmidt number for k (=0.5)
σ_ω	turbulent Prandtl-Schmidt number for ω (=0.5)
σ_P^g	Planck opacity for radiation in group g
σ_R^g	Rosseland opacity for radiation in group g
ω	specific dissipation rate of turbulent kinetic energy

Subscripts:

a	ablated material
bulk	bulk plasma material
e	electrons
fs	freestream value
H	heavy particles (=ions + neutral atoms)
i	x-index for mesh points
ion	ions
isp	species index
ist	ionization state
j	y-index for mesh points
n	neutral atoms
R	radiation
T	turbulent
w	wall
x	streamwise direction
y	normal direction

1. INTRODUCTION

Plasma-surface interactions are of great interest for the design and modeling of devices in which there is direct contact between a plasma and interior surfaces. Examples of such devices are electric launchers, which are used for purposes ranging from injecting fuel into fusion reactors to launching payloads either for military or space applications, and future large fusion devices such as tokamaks, in which the plasma impacts on the first wall, limiters and divertors. Modeling of plasma-surface interactions requires a detailed analysis of the energy transfer physics near the plasma-surface interface and the mixing processes between ablated surface material species and the bulk plasma. The purpose of this research is to develop a model to investigate these interactions in devices where the plasma flows along a surface, such as electrothermal plasma launchers. Factors that must be considered in modeling such systems include surface ablation, turbulence and radiant energy transfer.

Experimental results suggest that turbulence enhances energy transport through the turbulent mixing of hot outer fluid with the cooler fluid near the surface[2,3]. Previous models have not combined radiant energy transport with turbulent convection in a self-consistent manner. Codes such as MAGFIRE[10,11] have shown that radiation transport from the plasma is the dominant mechanism responsible for heating and ablating plasma-facing materials, and that conduction

has a small effect. One goal of this research is to resolve the roles of turbulence and radiation on energy transport to the surface.

Another goal of this research is to investigate thermal shielding that may occur when there is a large heat flux to the surface. The vapor shielding effect, described by Gilligan et al.[7], occurs when vaporized material adjacent to a surface absorbs much of the incident energy and thereby reduces the heat flux incident on the surface. Any increase in energy transport to the surface via turbulent convection or radiation is expected to be self-limiting due to the increased shielding effect. In electrothermal-chemical launchers, the burn rate may be limited by such shielding mechanisms at the combustion flame temperature. Recent work by Eapen[5] suggests that most or all of the shielding seen in electrothermal launcher experiments and previous computer codes may be the result of hydrodynamic effects rather than absorption of incident energy by a near-wall vapor layer.

As a part of this research, the 2-D code TURBFIRE has been developed. TURBFIRE models boundary layer plasma flow and predicts mass evolution rates at the plasma-surface interface. This code will aid in the understanding of thermal shielding of the surface and the effects of turbulence and radiation on energy transport to the surface. The system has been modeled using fluid boundary layer equations, which include a two-equation (k-ω) model for turbulence, coupled with multi-group thermal radiation transport. TURBFIRE is the first code to model

turbulence, radiation and ablation in a self-consistent manner for plasma flow along a surface.

Several aspects of the numerical simulation used in this research differ from methods traditionally used in computational fluid dynamics (CFD) codes. In order to model plasma flow at high temperature and pressure, traditional models had to be adapted in several ways. First, the energy equation was written in terms of internal energy. It was found that using an energy equation written in terms of temperature lead to poor convergence properties due to large changes in heat capacity when ionization becomes significant. Previous turbulent flow codes have not included plasma models for heat capacity ($C_V=dU/dT$) or thermal conductivity. Additionally, the energy equation was discretized in a manner more implicit than in typical CFD codes. This modification was found to be necessary to achieve convergence when modeling plasma flow.

Boundary conditions for the k-ω turbulence model also had to be adapted to plasma flow. CFD codes generally use measured values of k_{fs} and ω_{fs} for the free stream boundary conditions, but such experimental data is not available for electrothermal plasma launchers. Instead, zero-gradient boundary conditions were used for k and ω at the free stream ($dk/dy=d\omega/dy=0$). These boundary conditions were first tested for low temperature flows, for which they were found to be equivalent to the traditional constant-value boundary conditions.

Some limitations of this research are the absence of magnetic fields, which would be needed to model electromagnetic launchers or magnetic fusion devices, a surface combustion model (necessary for modeling electrothermal-chemical launchers), and the ability to model flow separation, which becomes important with very high rates of ablation.

In Chapter 2, relevant theory and previous models are discussed. Sections are devoted to ablation-controlled arcs and fluid flow modeling. Chapter 3 presents the models of fluid dynamics and radiation transport, their implementation in the TURBFIRE code, and a discussion of model assumptions. Chapter 4 presents and discusses code results, including benchmark cases and runs for plasma conditions. Conclusions and Recommendations for future work are presented in Chapter 5. Finally, a description of the TURBFIRE code and sample input and output files are presented in the Appendices.

2. LITERATURE REVIEW

2.1 Ablation-Controlled Arcs and the Vapor Shielding Effect

Ablation-controlled arcs are high-density, low temperature discharges formed through arc-induced wall ablation in electrothermal launchers and plasma switches. Many of the results presented in this study are for code runs that simulate electrothermal launchers. There are two reasons for this. First, electrothermal launchers are ideal for studying plasma-surface interactions under conditions similar to those occurring in a wide variety of devices. Second, experimental results are readily available, since the author's colleagues at N.C. State University have used the SIRENS electrothermal facility to study plasma-surface interactions since the mid-1980's[1,2,3,7]. A simplified schematic diagram of SIRENS source and barrel sections is shown in Figure 2.1.

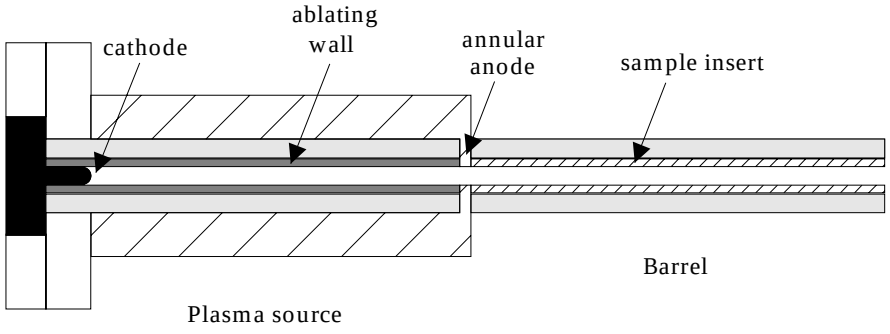

Figure 2.1: Schematic of the Plasma Source and Barrel Sections of SIRENS

Two main components of most electrothermal launchers are the plasma source and the barrel. In the source, an arc is created by releasing energy from a capacitor across two electrodes. The arc ablates the lining of the source section (often a polycarbonate material), creating a high-density, low-temperature plasma, which rapidly expands into and flows through the barrel. The plasma continues to accelerate in the barrel due to the large pressure gradient, and it can reach exit velocities of several kilometers per second. Electrothermal launchers range in size from very small (<0.5 cm bore diameter) pellet launchers used to fuel fusion experiments, to military anti-tank guns (>10 cm bore diameter).

Early models of ablation controlled arcs in capillaries were developed in the late 1970's and early 80's by Niemayer[24], Ibrahim[15] and Kovitya and Lowke[17]. In their research, the arc was found to effectively consist of two regions: a hot core with nearly constant temperature and a near-wall vapor that transmits some of the radiated core energy to the wall. These studies laid much of the groundwork for later simulations by showing that radiation is the dominant mechanism of energy transport (thus the flat temperature distribution in the core), and that the central plasma radiates as a blackbody at the plasma temperature. Beyond the common aspects of these studies, Ibrahim discussed the role of turbulence in the energy transport, and showed that turbulence increased the effective thermal conductivity by about an order of magnitude. Kovitya and Lowke built upon the models of Niemayer and Ibrahim by including a discussion of vapor shielding and estimating

(by comparison of their model to various experimental results) the fraction of energy transmitted through the vapor. Ruchti and Niemayer[30] also estimated energy transmission fractions by comparing experimental results to a two-zone model of ablation controlled arcs.

Loeb and Kaplan[19] developed an analytical model of electrothermal gun plasmas in a quasi-steady state, with the goal of optimizing parameters such as temperature, pressure, discharge energy and radius to attain higher exit velocities. They showed that the radial temperature profile only varies very close to the wall, and theorized that heat transport occurs primarily by radiation and turbulent convection.

In the late 1980's, Hahn and Gilligan[9,10] developed the MAGFIRE code to investigate vapor shielding and heat flux to the wall in electrothermal launchers and fusion reactors. MAGFIRE is a 1-D MHD code that models free expansion of ablated material from a surface exposed to a blackbody radiation source. The code models energy transport through the ablated vapor, using conservation equations and a multi-group radiation transport model. Hahn[10] found that radiation was the dominant mechanism of energy transport through the plasma, and that the energy transmission fraction (defined as the fraction of energy incident on the outer part of the ablated vapor that reaches the wall) for an iron wall ranged from 5% to 25%, depending for plasma core temperatures of 2-5eV. Hahn also showed that the time required to reach a quasi-steady state was much shorter (<10μs vs. >100μs) than the

time scale of a typical electrothermal gun discharge.

The radiation transport model used in both MAGFIRE and the present study was developed by Watrous et al.[33] for use in the ZPINCH code. It is based on a radiation transport equation derived by Zeldovich and Raizer[38] for conditions of local thermodynamic equilibrium (LTE). Taking advantage of the property that at LTE the radiation field changes little over the distance of a few mean free paths, Zeldovich and Raizier were able to relate the radiant energy flux vector, q, to the radiation energy density, E_R, using a diffusion approximation:

$$q(\nu) = -\frac{c\lambda(\nu)}{3}\nabla E_R(\nu) \tag{2-1}$$

The result was a radiation transport equation that is independent of the direction of propagation of the radiation:

$$\nabla \cdot \left[k_R(\nu)\nabla E_R(\nu)\right] = \frac{c}{\lambda(\nu)}\left[E_{R,p}(\nu) - E_R(\nu)\right] \tag{2-2}$$

The flux-limited diffusion model used in ZPINCH modifies the radiation transport model by restricting the maximum allowable flux that can flow from one numerical mesh zone to the next. Use of a flux limit extends the validity of the model to more optically thin regions than could otherwise be modeled. Hahn[10]

showed that limiting the flux to $(c/2)E_R(\nu)$ gave the best agreement with experimental results for an electrothermal launcher. The physical meaning of the flux limit is evident from the definitions of the spectral radiation density and flux:

$$E_R(\nu) = \frac{1}{c}\int_{4\pi} I(\nu)\,d\Omega \quad \text{and} \quad \underline{q}(\nu) = \int_{4\pi} I(\nu)\,\underline{\Omega}\,d\Omega \tag{2-3}$$

from which it can be seen that a flux of $q(\nu)=(c/4)E_R(\nu)$ corresponds to isotropic radiation, and $cE_R(\nu)$ corresponds to completely anisotropic (unidirectional) radiation. The value of $(c/2)E_R(\nu)$ can be justified by the argument that in areas where the ET plasma is less optically thick, radiation will be somewhat anisotropic and tend to stream toward the surface.

Tables of opacities and ionization states used in MAGFIRE were calculated by the MIXERG code, which was developed by Peterson and Moses[29] in the early 1980's. MIXERG calculates Rosseland and Planck opacities (essentially mass attenuation coefficients) for a mixture of up to five gases. Absorption mechanisms included in the calculations are photoionization, inverse Bremsstrahlung, bound-state to bound-state atomic line absorption and absorption by plasma waves. Thomson scattering is included only in the Rosseland opacities, because these are used in the calculation of radiation conductivity, while the Planck opacities are used to calculate absorption and emission coefficients. MIXERG chooses between

the Saha and Coronal ionization models based on plasma conditions, and uses a smooth transition between the two to avoid sharp changes which could affect equation of state calculations. The MIXERG code was also used to calculate opacities for the present study.

Improvements in computers in the 1990's have allowed for more detailed models of ablation controlled arcs. Coffee[4] developed a 2-D fluid dynamics model of the combustion chamber of an electrothermal-chemical gun, which included a k-ε model for turbulence and a simple combustion model. Gilligan and Mohanti[8] developed the 0-D, time dependent code ZEUS to simulate conditions in an ET gun source and investigate nonideal effects. More recently, 1-D, time-dependent models of discharges in ablative capillaries have been developed by, Hurley[14] and Zoler et al.[39] One conclusion of Zoler's research was that plasma parameters quickly reach a quasi-steady state, so the use of steady state models is justified for electrothermal gun plasmas.

Ngo[25] combined a 1-D, time-dependent fluid dynamics model with 2-D energy transport to model an ET gun plasma source. This pseudo-two-dimensional model allowed his TITAN code to calculate both axial behavior of the plasma and radial profiles of temperature and current density. TITAN also included non-ideal effects and a simple model for radiation transport. Ngo's results showed good agreement with the SIRENS experiment, and he showed that the plasma produced by SIRENS meets the criteria for LTE.

Eapen[5] created a 2-D time dependent model to investigate ablation and plasma hydrodynamics in the barrel of an ET gun. He found that ablation reduces the energy flux to the wall even when radiation transport is neglected. The TURBFIRE code can be used to further investigate the magnitude of this effect, which Eapen termed hydrodynamic thermal shielding.

Much work has also been done to model ablation of plasma-facing components in fusion devices. Throughout the 1980's and 90's, Hassanein et al.[11,12,13] have investigated surface erosion during disruptions in tokamaks. Hassanein's early work looked at melting and ablation of the surface material, and the work has progressed to a heat conduction model with two moving boundaries (plasma-melted surface and molten surface material-solid), that includes the effects of disruption length, vapor shielding and wall protection with thin coatings. Bourham and Gilligan[2] have also applied results of their electrothermal gun experiments and modeling to the case of disruptions.

2.2 Turbulent Flow Modeling

As a model of turbulent boundary-layer flow is an integral part of the present study, some background on the modeling of fluid flow is presented. Laminar boundary-layer flow is well understood • an outline of a simple model and its finite difference solution scheme can be found in the textbook by White[34] • so this section will focus on turbulent flow modeling.

The modeling of turbulent flow is an area of much research and continuing model improvement, even for simple geometries such as flow on a flat plate. Two inherent properties of turbulent flow are irregularity and enhanced mixing due to eddies. Because of these properties, it is computationally intensive to directly model even the largest eddies, and a complete model of the turbulence may never be accomplished. Instead, models have been developed that look at the average properties of the flow.

Such models are based on the work of Boussinesq in the late 1800's and Prandtl in the early 1900's[31,34]. Boussinesq used a gradient diffusion model to describe the increased shear stress due to turbulence:

$$\tau_{xy,T}=\mu_T dU/dy \qquad (2\text{-}4)$$

This expression treats momentum transport by turbulent eddies in a manner analogous to the molecular transport of momentum. While the expression is not

exact, it is the basis for most turbulence modeling even today.

Prandtl[31,34] proposed relationships between the eddy viscosity, a length scale and turbulent kinetic energy (k),

$$\mu_T=\rho k^{1/2}\ell \tag{2-5}$$

and developed an equation for the transport of turbulent kinetic energy. A modified version of this equation is used today in both one-equation (turbulent kinetic energy) models and two-equation models, in which it is combined with a second equation describing the transport of either a scale length or dissipation of turbulent energy.

While one-equation models can predict very simple flows fairly well, they are not useful without some prior knowledge of the flow, which is necessary to specify a scale length ℓ. Even in the simplest cases, turbulent eddies with a wide range of sizes are present, so it is not obvious what scale length should be specified. Kolmogorov[22] developed the first two-equation model (k-ω) in the 1940's, and a k-ε model was developed for use on computers by Jones and Launder in 1968[16]. These models used dissipation rates rather than scale length, based on the idea that, like turbulent kinetic energy, dissipation is a fundamental property of turbulence. In all turbulent flows, dissipation occurs through a process of energy being transferred from the largest eddies down to the smallest, where it is dissipated as heat. Scale

length, ε and ω are related by the expressions:

$$\mu_T = \rho k^{1/2} \ell = \rho k / \omega = \rho C_\mu k^2 / \varepsilon \quad \text{and} \quad \omega = \varepsilon / \beta^* k. \tag{2-6}$$

Thus ω can be described as the rate of dissipation per unit turbulent kinetic energy.

The k-ε model was the two-equation turbulence model of choice until Wilcox[35] further developed the k-ω model in the early 1990's. Wilcox's k-ω offered significant improvements over the k-ε model in terms of accuracy, and resolved difficulties in applying the k-ε model near walls. The accuracy of two-equation models for flow along a flat plate have been compared by Patel et al.[28] and by Wilcox[36], who found that the k-ω model is superior to k-ε models for predicting flow along a flat plate, and that k-ε model predictions are inaccurate in the presence of even a mild adverse pressure gradient.

Despite the success of two-equation models, much of their development has been based on dimensional analysis rather than derivation from the fundamental physics. For this reason, all of the models involve closure coefficients, which use experimental observations to approximate unknown correlations in terms of known flow properties[16,18,35]. While appropriate values for these closure coefficients have been determined for conventional fluid flow on a flat plate, it is not clear that these values can be used to model flows with the high temperatures, high pressures and large temperature gradients present in electrothermal launchers and other plasma

devices. Reliance on these conventional values of the closure coefficients may be a significant source of error in the present research. This concern is addressed in part in Section 4.3 of the Results.

3. METHOD

3.1 Fluid Dynamics Model

3.1.1. Geometry and Boundary Conditions

Since the purpose of the current research is to investigate near-wall phenomena, the geometry has been simplified to the case of plasma flow in a boundary layer along a flat plate. The geometry is shown in detail in Figure 3.1.

Boundary conditions for each of the variables are presented in Table 3.1. Inlet conditions are presented for both constant (for code runs started at Point A in Figure 1) and profile (runs started at Point B) input. Boundary conditions at the wall and the free stream are also presented. Some of the boundary conditions will be discussed in more detail below, in the sections that present the appropriate equations.

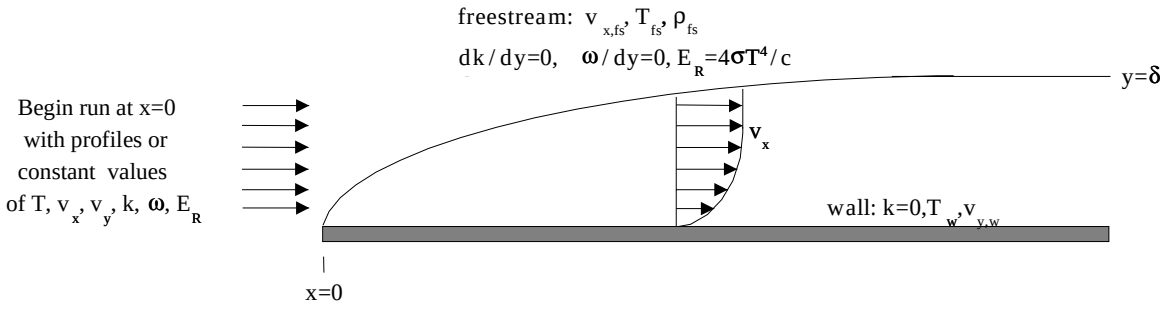

Figure 3.1: Schematic of a boundary layer on a flat plate

Table 3.1: Boundary Conditions for the System of Equations

Variable	inlet b.c. (x=0)		wall b.c. (y=0)	freestream b.c (y=δ)
	constant	profile		
plasma x-velocity	$v_x = v_{x,fs}$	v_x profile	$v_x = 0$	$v_x = v_{x,fs}$
plasma y-velocity	$v_y = v_{y,a} = \frac{f_{abl} q''}{H_{sub} n_a}$ at wall, =0 elsewhere	v_y profile	$v_y = v_{y,a} = \frac{f_{abl} q''}{H_{sub} n_a}$	$v_y = 0$
temperature	$T = T_{fs}$	T profile	$T = T_{wall}$	$T = T_{fs}$
density	ρ(P,T)	ρ (P,T)	ρ (P,T)	ρ (P,T)
ablated species mass fraction	x=0	x=0	$x = x_{wall}$	x=0
turbulence KE	k=0	k profile	k=0	dk / dy=0
turbulence KE dissipation rate	ω=0	ω profile	$\omega = \frac{N_\omega \nu}{y^2}$ (for all $y^+ < 2.5$)	dω / dy=0
radiation energy density	$E_R = \sum_{g=1}^{20} E_R^g = \frac{4}{c}\sigma T^4$	E_R profile	Partial current: $q_+'' = \sigma T^4$	$E_R = \sum_{g=1}^{20} E_R^g = \frac{4}{c}\sigma T^4$

3.1.2 Conservation Equations

The conservation equations are written in terms of mean quantities. They were obtained from the conservation equations for laminar flow by dividing velocities, internal energy, pressure and densities into densities into an average value and a fluctuating part for each[18], for example $p = \bar{p} + p'$, where $\bar{p}$ is the time-average of pressure at a given point and p' is its fluctuating component. To simplify the resulting conservation equations for the averaged quantities, the velocities and internal energy are written in terms of mass-weighted means rather than their time averages: $v_x = \tilde{v}_x + v_x''$, where the mass weighted mean $\tilde{v}_x \equiv \overline{\rho v_x}/\bar{\rho}$, and a straight bar indicates a time-average.

After substituting the above expressions for density and velocities, the continuity equation can be expressed as:

$$\frac{\partial(\bar{\rho}_i \tilde{v}_x)}{\partial x} + \frac{\partial(\bar{\rho}_i \tilde{v}_y)}{\partial y} = 0 \qquad (3\text{-}1)$$

where the index i denotes either the bulk plasma or the ablated material. It may be noted that there is no ablation term in this equation. Instead, ablation is accounted for in the wall boundary condition, as shown in Figure 3.1, which specifies that a fraction f_{abl} of the energy incident on the wall results in wall surface ablation. Since much of the incident energy is conducted into the wall or goes into heating, it is

expected that not all of the incident energy goes to ablating surface material, and therefore the energy fraction towards ablation must satisfy $0<f_{abl}<1$. Values used for f_{abl} will be discussed in the Results section.

The conservation equations for momentum in the x- and y-directions are expressed as:

$$\overline{\rho}\tilde{v}_x \frac{\partial \tilde{v}_x}{\partial x} + \overline{\rho}\tilde{v}_y \frac{\partial \tilde{v}_x}{\partial y} = -\frac{\partial P}{\partial x} + \frac{\partial}{\partial y}\left[(\mu + \mu_T)\frac{\partial \tilde{v}_x}{\partial y}\right] - \frac{2}{3}\frac{\partial \overline{\rho} k}{\partial x} \tag{3-2}$$

$$\frac{\partial P}{\partial y} = 0 \tag{3-3}$$

where ρ is the mixture density. The left-hand side of the x-momentum equation represents convective changes in the momentum flux. The first and third terms on the right-hand side represent changes in momentum flux due to pressure forces and turbulent convection. The second term represents the changes due to viscous shear stress and the apparent shear stress caused by turbulent fluctuations, known as the Reynolds stress.

The y-momentum equation has been simplified to the form above in accordance with Prandtl's boundary layer approximation[31,34]. While this simplification was originally derived for laminar flow, the effect of turbulence on the

y-direction pressure gradient has been shown to be small, and it is generally neglected[34,35].

The conservation equation for internal energy is expressed as:

$$\bar{\rho}\tilde{v}_x \frac{\partial \tilde{U}}{\partial x} + \bar{\rho}\tilde{v}_y \frac{\partial \tilde{U}}{\partial y} = -P\frac{\partial \tilde{v}_x}{\partial y} + \mu\left(\frac{\partial \tilde{v}_x}{\partial y}\right)^2 + \beta^* \bar{\rho}\omega k + \frac{\partial}{\partial y}\left[\left(\frac{\lambda}{C_V} + \frac{\mu_T}{Pr_T}\right)\frac{\partial \tilde{U}}{\partial y}\right]$$

$$- \sum_{g=1}^{20} c\bar{\rho}\sigma_P^g\left(E_{RP}^g - E_R^g\right) \qquad (3\text{-}4)$$

The left-hand side of the energy equation represents convective changes in the energy density. The first three terms on the right-hand side represent work done by the fluid, dissipation of energy due to friction, and turbulent dissipation (the rate at which turbulent kinetic energy is converted to thermal energy, respectively. The fourth term represents the transport of energy due to conduction and turbulent diffusion. The final term represents the transport of energy due to radiation, and consists of terms for the absorption and emission of radiation by the plasma. A constant value of the turbulent Prandtl number, Pr_T=0.89, has been shown to be satisfactory for shock-free flows[35].

Equations for the transport of turbulent kinetic energy and its specific dissipation rate, ω, are given by:

$$\overline{\rho}\tilde{v}_x \frac{\partial k}{\partial x} + \overline{\rho}\tilde{v}_y \frac{\partial k}{\partial y} = \mu_T \left(\frac{\partial \tilde{v}_x}{\partial y} \right)^2 - \beta^* \overline{\rho} \omega k + \frac{\partial}{\partial y} \left[(\mu + \sigma_k \mu_T) \frac{\partial k}{\partial y} \right] \quad (3\text{-}5)$$

$$\overline{\rho}\tilde{v}_x \frac{\partial \omega}{\partial x} + \overline{\rho}\tilde{v}_y \frac{\partial \omega}{\partial y} = \alpha \frac{\omega}{k} \mu_T \left(\frac{\partial \tilde{v}_x}{\partial y} \right)^2 - \beta^* \overline{\rho} \omega^2 + \frac{\partial}{\partial y} \left[\left(\mu + \sigma_\omega \mu_T \right) \frac{\partial \omega}{\partial y} \right] \quad (3\text{-}6)$$

where α=0.556, β^*=0.09, σ_k=0.5,and σ_ω=0.5 are empirical constants that have been found to be accurate for simple geometries[18,35]. In each equation, the left-hand side represents convective changes in k and ω. On the right hand side of equation 3-5, the first term represents production of turbulent kinetic energy (the rate of energy transfer from the mean flow to turbulence), the second, dissipation (the rate at which k is converted into thermal energy), and the final term the rates of viscous and turbulent diffusion of k. The terms on the right hand side of equation 3.6 have analogous interpretations[35].

Numerical solution of the k-ω equations near the wall presents a problem, since $d\omega/dy$ is large and rapidly changing in this region. To overcome this problem, a solution method prescribed by Wilcox[35] has been adopted. The equation for ω is solved between the freestream and a point near the wall ($y^+ \approx 2.5$). At points closer to the wall, the relationship $\omega = \frac{N_\omega \nu}{y^2}$ is used, where $N_\omega = 2/\beta^*$. Since the turbulent kinetic energy equation is well behaved near the wall (where k=0), it is solved all the

way to the wall.

The equation of state is written for multiple species as:

$$\overline{P} = \sum_{isp=1}^{N_{species}} \overline{P}_{isp} = \sum_{isp=1}^{N_{species}} \overline{n}_{isp} k_B \tilde{T}(1 + \overline{z}_{isp}) \tag{3-7}$$

where i_{sp} is the index for species.

An equation of state is also needed to relate temperature to internal energy:

$$\tilde{U} = \sum_{isp=1}^{N_{species}} \frac{\overline{\rho}_{isp}}{\overline{\rho}} \tilde{U}_{isp} = \sum_{isp=1}^{N_{species}} \frac{\overline{\rho}_{isp}}{\overline{\rho}} \left[\frac{3}{2} k\tilde{T}(1 + \overline{z}_{isp}) + \overline{I}_{isp} \right] \tag{3-8}$$

Once the energy equation has been solved, equation 3-8 can be used to calculate the temperatures across the boundary layer.

The Saha equation, which describes the populations in each ionization state, is given by:

$$\frac{n_e n_{ist+1}}{n_{ist}} = 2 \frac{g_{ist+1}}{g_{ist}} \left(\frac{2\pi m_e kT}{h^2} \right)^{3/2} \exp\left(-\frac{I_{ist}}{k_B T} \right) \tag{3-9}$$

where ist=1 denotes neutral, ist=2 singly ionized, and so on. To calculate the

average ionization state for a species, the Saha equation is solved for the six most populous states, and the average ionization state is given by:

$$\bar{z}_{isp} = \frac{\sum_{ist} \left[n_{ist} \cdot (ist - 1) \right]}{\sum_{ist} n_{ist}} \tag{3-10}$$

Since the Saha equation contains the total electron density, the average ionization states of separate species are interdependent. For this reason, the Saha equation must be solved iteratively when there is more than one plasma species.

3.1.3 Fluid properties

The plasma viscosity can be written as the sum of the viscosities due to neutral atoms and to ions[14]:

$$\mu = \mu_n + \mu_{ion}$$

$$= \frac{1}{3} \rho_n \lambda_n v_{th,n} + \frac{1}{3} \rho_{ion} \lambda_{ion} v_{th,ion} \tag{3-11}$$

The mean free paths are given by[21]:

$$\lambda_n = \frac{1}{n_n \bar{Q}_{en}} \text{ and } \lambda_{ion} = \frac{25\pi\varepsilon_0^2 (kT)^2}{Z^4 n_{ion} e^4 \ln(1+1.4\Lambda_m^2)^{1/2}} \tag{3-12}$$

where the modified Coulomb logarithm is used to account for non-ideal effects, and, assuming the ions and neutral atoms have the same temperature, the thermal velocities are given by:

$$v_{th,n} = v_{th,ion} = \sqrt{k_B T/m} \tag{3-13}$$

Since free electrons are much more mobile than ions and neutral atoms, they are responsible for nearly all of the heat conduction. The thermal conductivity can be written in terms of the electron-ion and electron-heavy particle collision frequencies[20]:

$$k_{th} = \frac{2.4}{1+\bar{\nu}_{eion}/\sqrt{2}\bar{\nu}_{eH}} \frac{k_B^2 n_e T}{m_e \bar{\nu}_{eH}} \tag{3-14}$$

where the collision frequencies are related by the expression

$$\bar{\nu}_{eH} = \bar{\nu}_{eion} + \bar{\nu}_{en} \tag{3-15}$$

At temperatures too low for significant ionization, thermal conduction no longer occurs primarily through the motions of free electrons, so the thermal conductivities calculated by the above formula become unreasonably small. To accurately model conduction near the wall, empirical models are used for each species. These are shown in Table 3.2. For cases with ablation, the thermal conductivity for the mixture is calculated using a harmonic mean:

$$k_{th,mix} = \frac{2k_{th,1}k_{th,2}}{k_{th,1} + k_{th,2}} \tag{3-16}$$

In the TURBFIRE code, the thermal conductivity is calculated using both models near the wall, and the value from the low temperature models are used up to temperatures where the high temperature model gives a larger value.

Table 3.2 Thermal Conductivities for Plasma Species at Low Temperatures[37]

species	thermal conductivity [W/m-K]
iron	$k_{th} = 0.0235 - T * 4.3192 * 10^{-6} + T^2 * 4.1782 * 10^{-9}$
carbon	$k_{th} = -01914 + T * 4.9735 * 10^{-5} + T^2 * 4.5834 * 10^{-10}$

3.2 Radiation Transport Model

Radiation transport enters the model through the last term in the energy equation. A radiation transport equation (3-17) has been derived using flux limited diffusion theory, which has been shown to be valid for electrothermal launcher plasmas[10].

$$\frac{\partial}{\partial y}\left[K_R^g \frac{\partial E_R^g}{\partial y} \right] = c\rho\sigma_P^g \left(E_{RP}^g - E_R^g \right) \tag{3-17}$$

where K_R^g is the radiation conductivity[33] for radiation in frequency group g, $K_R^g = \frac{c}{3\bar{\rho}\sigma_g^R}$, E_{RP}^g is the equilibrium radiation density of a plasma at temperature T, $E_{RP}^g = \frac{c}{4}\sigma T^4$, and Rosseland and Planck opacities are obtained from the MIXERG code, which is discussed in the Literature Review. This equation is solved for 20 frequency groups, using finite difference techniques. Radiation transport in the flow direction is neglected since the streamwise temperature gradient is small.

An important assumption in deriving the radiation transport equation is that the diffusion approximation is valid, and thus that the radiation flux is related to the radiation energy density by the relation:

$$q(\nu) = -\frac{\lambda_\nu c}{3} \nabla E_R(\nu) \tag{3-18}$$

where λ_ν is the radiation absorption mean free path for frequency ν. Equation 3-17 is only valid for plasma at local thermodynamic equilibrium (LTE), in which density is high enough that collisional processes dominate. To account for cases in which the plasma is not dense enough to justify the approximation of LTE, a flux limit of $(c/2)*E_R^g$ is implemented. As discussed in the Literature Review, this modifies the diffusion theory to simulate free streaming in optically thin plasmas, and it has been shown to be satisfactory for modeling electrothermal gun plasmas[9,10,20]. The radiation transport model should be modified, however, if the TURBFIRE code is to be used for cases where LTE is not valid over large regions of the computational domain.

Consistent with diffusion theory, a partial current boundary condition has been used for the radiation energy flux from the wall:

$$q_R^{g+} = \left(\frac{c}{4} E_R^g - \frac{K_R^g}{2} \frac{dE_R^g}{dy} \right)_{wall} \tag{3-19}$$

where the plus sign ($^+$) denotes the positive-y direction, from the wall into the plasma. By assuming that the wall radiates as a blackbody at the wall temperature ($q_R^{g+} = \frac{c}{4} E_{RP}^g(T_w)$), equation 3-19 can be rewritten:

$$q''_w = \left(- K_R^g \frac{dE_R^g}{dy} \right)_w = -\frac{c}{4}\left(E_{RP}^g - E_R^g \right) \qquad (3\text{-}20)$$

which can be used in the discretized version of the radiation transport equation at the wall.

3.3 Computer Implementation

The system of equations is solved using a semi-implicit finite difference method. To simplify description of the discretization scheme, it is convenient to write equations 3-2,4,5,6 and 17 in the form of a general PDE:

$$\alpha\left(\overline{\rho}\tilde{v}_x\frac{\partial\Phi}{\partial x}+\overline{\rho}\tilde{v}_y\frac{\partial\Phi}{\partial y}\right)=\frac{\partial}{\partial y}\left(\Gamma\frac{\partial\Phi}{\partial y}\right)+a\left(\frac{\partial b}{\partial x}\right)^c+d\left(\frac{\partial e}{\partial y}\right)^f+S \tag{3-21}$$

The coefficients Φ, Γ, a, b, c, d, e, f and S are given for each equation in Table 3.3.

The equations are discretized such that the velocities, energy, temperature pressure and densities are evaluated at the node centers, while fluid properties such as viscosity and thermal conductivity are evaluated at the node boundaries. In this manner, the discretized form of this general PDE is written:

$$\begin{aligned}(\overline{\rho}\tilde{v}_x)_{i,j}&\left[\frac{\Phi_{i+1,j}-\Phi_{i,j}}{\Delta x}\right]+\frac{(\overline{\rho}\tilde{v}_y)_{i,j}}{2}\left[\frac{\Phi_{i,j+1}-\Phi_{i,j}}{\Delta y^+}+\frac{\Phi_{i,j}-\Phi_{i,j-1}}{\Delta y^-}\right]=\\ &\frac{\Gamma^+}{(\Delta y^+ +\Delta y^-)/2}\left[\frac{\Phi_{i+1,j+1}-\Phi_{i+1,j}}{\Delta y^+}\right]-\frac{\Gamma^-}{(\Delta y^+ +\Delta y^-)/2}\left[\frac{\Phi_{i+1,j}-\Phi_{i+1,j-1}}{\Delta y^-}\right]\\ &+a_{i,j}\frac{b_{i+1,j}-b_{i,j}}{\Delta x}+d_{i,j}\left[\frac{e_{i+1,j}-e_{i,j}}{\Delta y}\right]^f+S_{i+1,j}\end{aligned} \tag{3-22}$$

Table 3.3: Coefficients for the General PDE

equation	Φ	Γ	α	a	b	d	e	f	S
x-momentum	v_x	$\mu+\mu_T$	1	-1	P	-	-	-	$-\frac{2}{3}\frac{\partial\bar{\rho}k}{\partial x}$
energy	U	$\frac{\mu}{C_V}+\frac{\mu_T}{Pr_T}$	1	-	-	-P μ	v_x v_x	1 2	$\beta^*\bar{\rho}\omega k+\sum_{g=1}^{20}c\bar{\rho}\sigma_P^g\left(E_{RP}^g-E_R^g\right)$
turbulence KE	k	$\mu+\sigma_k\mu_T$	1	-	-	μ_T	v_x	2	$-\beta^*\bar{\rho}\omega k$
turbulence dissipation	ω	$\mu+\sigma_\omega\mu_T$	1	-	-	$\alpha\frac{\omega}{k}\mu_T$	v_x	2	$-\beta^*\bar{\rho}\omega^2$
radiation transport	E_R^g	K_R^g	0	-	-	-	-	-	$-c\bar{\rho}\sigma_P^g\left(E_{RP}^g-E_R^g\right)$

and the discretized continuity equation is given by:

$$\frac{1}{2}\left[\frac{(\overline{\rho}\tilde{v}_x)_{i+1,j}-(\overline{\rho}\tilde{v}_x)_{i,j}}{\Delta x}+\frac{(\overline{\rho}\tilde{v}_x)_{i+1,j-1}-(\overline{\rho}\tilde{v}_x)_{i,j-1}}{\Delta x}\right]+\frac{(\overline{\rho}\tilde{v}_y)_{i+1,j}-(\overline{\rho}\tilde{v}_y)_{i+1,j-1}}{\Delta y^-}=0 \qquad (3\text{-}23)$$

Rather than using a simple forward difference for the first term of the continuity equation, it has been written at level j+1/2. This is necessary to improve numerical accuracy[34].

The discretized equations are cast into matrix form by grouping terms at each mesh point. They are solved in the order shown in Table 3.4, using a forward-marching procedure starting at x=0. To achieve convergence, it is necessary to solve the equations in three nested iteration loops. Because an outer iteration loop has been implemented, values of the source term, S, in the general PDE are at x-index i+1.

Table 3.4: Solution Scheme, showing equations solved in each of the three nested iteration loops.

iteration loop			Equation			solve for
outer			Solve radiation transport equation			E_R^g
outer	energy			Solve energy equation		U
outer	energy	inner			Solve T/U equation of state	T
outer	energy	inner			Solve Saha equation	$\bar{z}_a$ & $\bar{z}_b$
outer	energy	inner			Solve equation of state	ρ
outer	energy	inner			Solve ablated species continuity equation	ρ_{abl}
outer			Solve x-momentum equation			v_x
outer			Solve continuity equation			v_v
outer			Solve k & ω equations			k & ω

3.4 Discussion of Model Assumptions

The radiation transport model has been derived under the assumptions that the plasma is in local thermodynamic equilibrium (LTE) and the diffusion approximation is valid. Due to the relatively high density and low temperatures near the wall of an ablative system, collisional ionization and three-body recombination dominate over other forms of ionization and recombination. Ions and electrons have a Maxwellian distribution, so the plasma can be described by the total density and single temperature. Hahn[10] and Ngo[25] have confirmed that the assumption of LTE is valid for the temperatures and densities present in an electrothermal launcher. Additionally, Murali[23] performed a series of experiments in which he used different materials (Cu-Al or Cu-W) for the barrel of an electrothermal launcher. His spectral analysis showed the same temperature for all species, indicating that the plasma was at LTE. A quantitative condition for LTE is that the electron density and temperature satisfy the relation[29] $n_e > 10^{22} T_{eV}^{7/2}$ [m^{-3}]. In order to test the validity of the LTE approximation, this relation will be plotted for several of code runs presented in the results (see Figure 4.18). Although the conditions for LTE are met for electrothermal plasmas, they should be investigated if other plasma devices are to be modeled with the TURBFIRE code.

For the diffusion approximation to be valid, radiation scattering mean free paths must be less than the dimensions of interest. While the maximum radiation mean free paths are on the same order as the mesh spacing, the mean free paths for

most frequencies are much smaller. Past experience with the diffusion approximation has shown that the use of a flux limit yields good results for electrothermal plasmas[11].

Plasma flow has been modeled using a hydrodynamic model. Implicit in this model is the assumption that charges balance in any volume of interest (quasi-neutrality), which is valid as long as the fluid motion being considered has a scale much larger than the Debye radius. For conditions near the freestream and the wall of a typical electrothermal gun plasma:

$$\lambda_D = \sqrt{\frac{\varepsilon_0 kT}{n_e e^2}} \approx \begin{cases} 10^{-9}\text{m} & \text{for } n_e = 10^{25}\text{m}^{-3} \text{ and } T = 3\text{eV} \\ 2\text{x}10^{-7}\text{m} & \text{for } n_e = 10^{21}\text{m}^{-3} \text{ and } T = 10000\text{K} \end{cases} \tag{3-24}$$

so the assumption of quasi-neutrality can be used. As a result of LTE and quasi-neutrality, the plasma can be considered to behave as a single fluid, and electrodynamic effects on the plasma motion can be neglected. Because of the high density, however, the number of particles in a Debye sphere is not large, and nonideal effects on plasma thermal and optical properties should be considered. For this research, nonideality was only accounted for in the thermal conductivity, and even that used the relatively old model of Zoler and Cuperman. Future work should include up-to-date models of nonideal plasma effects on all plasma properties.

Prandtl showed that fluid flow near a surface could be divided into two regions, a thin boundary layer, in which viscous effects dominate, and an outer region, in which frictional forces are not important[31]. Since this study is primarily concerned with heat transport to the surface, and since mean free paths for both radiation and plasma particles are very short in the dense plasma near the surface, this study investigates flow only in the boundary layer. Implicit in the boundary layer model is the assumption that axial gradients of temperature, density, velocity and radiation energy density are much smaller than the gradients in the radial direction. This assumption is valid for electrothermal launchers, since they have a diameter much less than the axial length (typically 0.4cm diameter and 10-12cm length for experimental devices such as SIRENS).

The TURBFIRE solution algorithm requires that the flow at a point depend only on quantities upstream. While this is certainly the case for laminar boundary-layer flow, its validity requires some discussion in the presence of turbulence, radiation and ablation. A forward marching scheme is commonly used to model turbulent flow on a flat plate[27,31]. Turbulent eddies can cause some flow of fluid from the downstream direction, but the results of codes using the forward-marching procedure have been shown to agree with experimental observations[36]. Radiation is inherently a process in which energy can be transported upstream. In the regions of interest to this project, however, the longest mean free paths are on the order of the mesh spacing (λ_{rad}<1mm), so the forward-marching procedure can be used. In

addition, except at the leading edge of the flat plate, temperature gradients are much greater in the cross-stream direction than in the axial direction, so radiation entering/exiting in the upstream direction will be nearly balanced by radiation entering/exiting in the downstream direction. Finally, in cases where the rate of ablation is very high, the flow can separate from the surface. TURBFIRE can not model the resulting upstream flow, so this imposes a limitation on the cases that can be run with the TURBFIRE code.

Other simplifying assumptions used in the fluid dynamics model are that the system being modeled quickly reaches a quasi-steady state, that the plasma is incompressible but thermally expandable, and that ablated material reaches equilibrium with the bulk plasma. Studies by Hahn[11] and Zoler et. al.[39] have shown that steady-state conditions are reached in a few microseconds in electrothermal launchers (compared to a typical shot, which lasts on the order of 100μs), so a steady state-model can be used to predict total energy transport to the surface and ablation over an entire shot.

The assumption of an incompressible, thermally expandable plasma is expected to lead only to small errors for subsonic flow, but it could lead to significant errors at higher velocities. The total pressure was set to a constant value throughout the region modeled, but density was allowed to change with temperature. Partial pressures of the ablated and bulk species were allowed to vary within the constraint that their sum was constant.

The ablation model assumes that material leaving the surface has the same temperature and velocity as the bulk plasma. The normal (y-direction) velocity at the wall is therefore dependent upon the amount of ablated material:

$$v_y = v_{y,a} = \frac{f_{abl} q''_{wall}}{H_{sub} n_a} \tag{3-25}$$

In the dense plasma near the surface, collision frequencies are very high, so temperature and momentum equilibrate very quickly. For a near-wall plasma with T=10000K, $n=10^{25} m^{-3}$ and $\bar{z}=0.001$ (so the average charge of the ions Z=1), it is necessary to look at equilibration times for ions and neutrals, since electrons equilibrate much more quickly than ions.

$$\tau_{ii} = \frac{(3)^{1/2} 6\pi\varepsilon_0^2 m_{ion}^{1/2} T^{1/2}}{Z^4 n_{ion} e^4 \ln(1+1.4\Lambda_m^2)^{1/2}} \approx 10^{-9} \text{seconds} \tag{3-25}$$

$$\tau_{nn} = \frac{\lambda}{v_{th}} \approx 10^{-11} \text{seconds} \tag{3-26}$$

While the fluid dynamics model has been tested against published results and other computer codes, there is some question of its validity for modeling plasmas. The area of most concern is the turbulence model. Values for the closure coefficients

in the k-ω equations have been studied for a wide range of flow conditions, but no work has been done to test their validity (or find appropriate values) for the high temperatures and large temperature gradients found in electrothermal launchers.

4. RESULTS

4.1 Test Cases for Fluid Flow

The TURBFIRE code has been run for laminar flow over a wide range of conditions. Velocity profiles for laminar flow are similar for any free-stream velocity, plate length or fluid. They can be reduced to a single profile (called the Blasius profile) by plotting velocity as a function of the dimensionless coordinate η, where:

$$\eta = y\sqrt{\frac{v_{x,fs}}{\nu_x}} \tag{4-1}$$

Results of a typical TURBFIRE run for laminar flow are presented in Figure 4.1. The velocity profiles for all laminar runs perfectly match the Blasius profile.

In contrast to laminar profiles, velocity profiles for turbulent flow depend on the free-stream velocity and do not collapse into a single curve such as the Blasius profile. When surface ablation and radiation are neglected, the turbulent boundary layer can be described by looking at its behavior in several regions[35]. Near the wall, viscous stresses dominate, and the velocity profile follows the linear relationship:

$$u^+ = y^+ \tag{4-2}$$

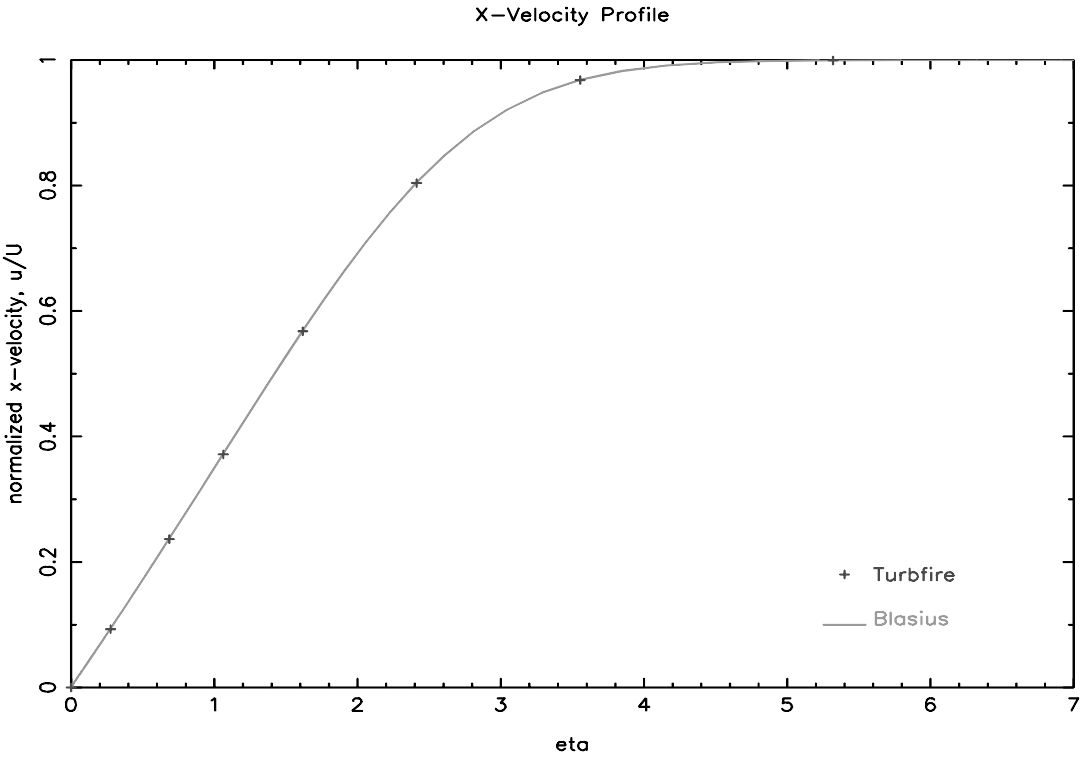

Figure 4.1 - TURBFIRE code results for laminar flow along a flat plate compared to the Blasius velocity profile

where the inner variables $u^+=yu_\tau/\nu$ and $y^+=u/u_\tau$ are used to put the profiles into dimensionless form, and the wall friction velocity is $u_\tau=(\tau_w/\rho)^{1/2}$. This "law of the wall", which is valid throughout the laminar velocity profile, is accurate for turbulent flow out to about $y^+=5$. Further away from the surface ($y^+>30$) turbulence dominates, and the profile follows the curve

$$u^+=5.61*\ln(y^+)+4.9. \qquad (4\text{-}3)$$

Equation 4-3 is known as the logarithmic law of the wall. Its functional form can be justified by an analysis of the turbulent shear stress, which shows that away from the wall $du^+/dy^+ \propto 1/y^+$, and thus that $u^+ = c_1 \log(y^+) + c_2$. The values of the constants c_1 and c_2 are empirical. It is important to note that equations 4.2 and 4.3 were used only as a comparison for turbulent flow benchmark. They are not used in the TURBFIRE code itself. Between the regions where the velocity profile follows equations 4.2 and 4.3 there is a transition, where the profile smoothly joins the two curves. Finally, at the outermost edge of the boundary layer the velocity profile is a function of the Reynolds number, and it rises above the logarithmic straight line. These four regions are evident in the results that follow for turbulent flow.

The EDDYBL[35] code has been run to provide benchmark cases to test TURBFIRE results for turbulent flow. In order to test the code over a range of temperature and pressure, three cases were chosen. A summary of the conditions for each is presented in Table 4.1.

Table 4.1 - Turbulent Benchmark Cases

	Description	T_{wall}	T_{fs}	**P**	$V_{x,fs}$
Case 1	Low $T_{fs} \cong T_w$, low pressure. (example case from Wilcox book)	240K	217K	0.12209bar	295m/s
Case 2	High $T_{fs} = T_w$, high pressure. (with $\bar{z} = 0$ and no radiation transport.)	30000K	30000K	500bar	295m/s
Case 3	low $T_{fs} > T_w$, low pressure.	300K	400K	1bar	295m/s

Results for the three benchmark cases are presented in Figures 4.2 through 4.4. The TURBFIRE velocity profiles agree well with those from EDDYBL for the first two cases, but there are significant differences in the Case 3 results. Specifically, TURBFIRE predicts slightly higher velocities than EDDYBL whenever the temperature of the fluid in the free-stream is significantly higher than the wall temperature. Temperature profiles for all three cases are slightly different from the EDDYBL results, so the difference in velocity profiles for Case 3 may be attributed to differences in viscosity between the two cases. Other possible causes for the differences between the results of the two codes are differences in boundary conditions, solution scheme and models for fluid properties. Since the details of these are not available for the EDDYBL code, the results are not expected to be identical. Additionally, the review paper by Patel et. al. presented velocity profiles for several variants of the k-ε and k-ω models, and these showed similar variations from the idealized log-law curve.

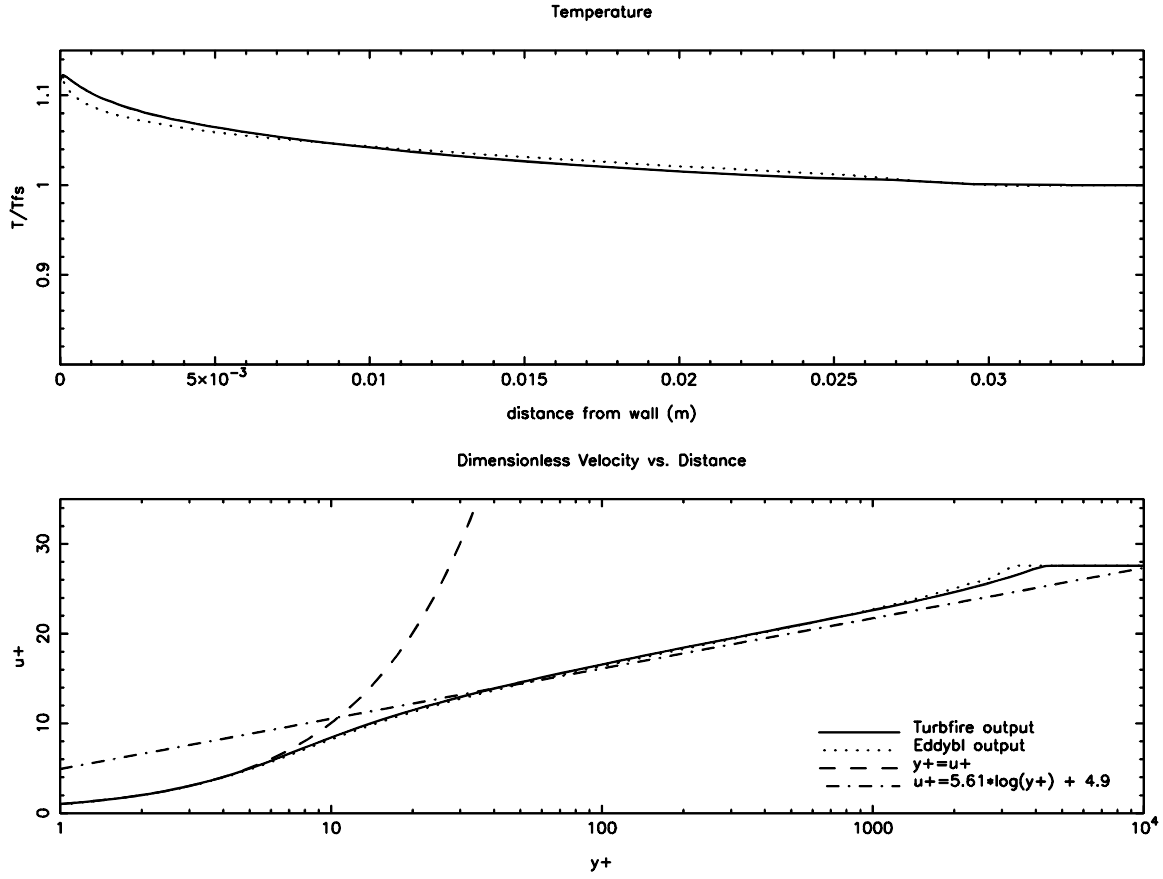

Figure 4.2 - Turbulent Benchmark Case 1: T_w=240K, T_{fs}=217K, P=0.12209bar, $v_{x,fs}$=295m / s.

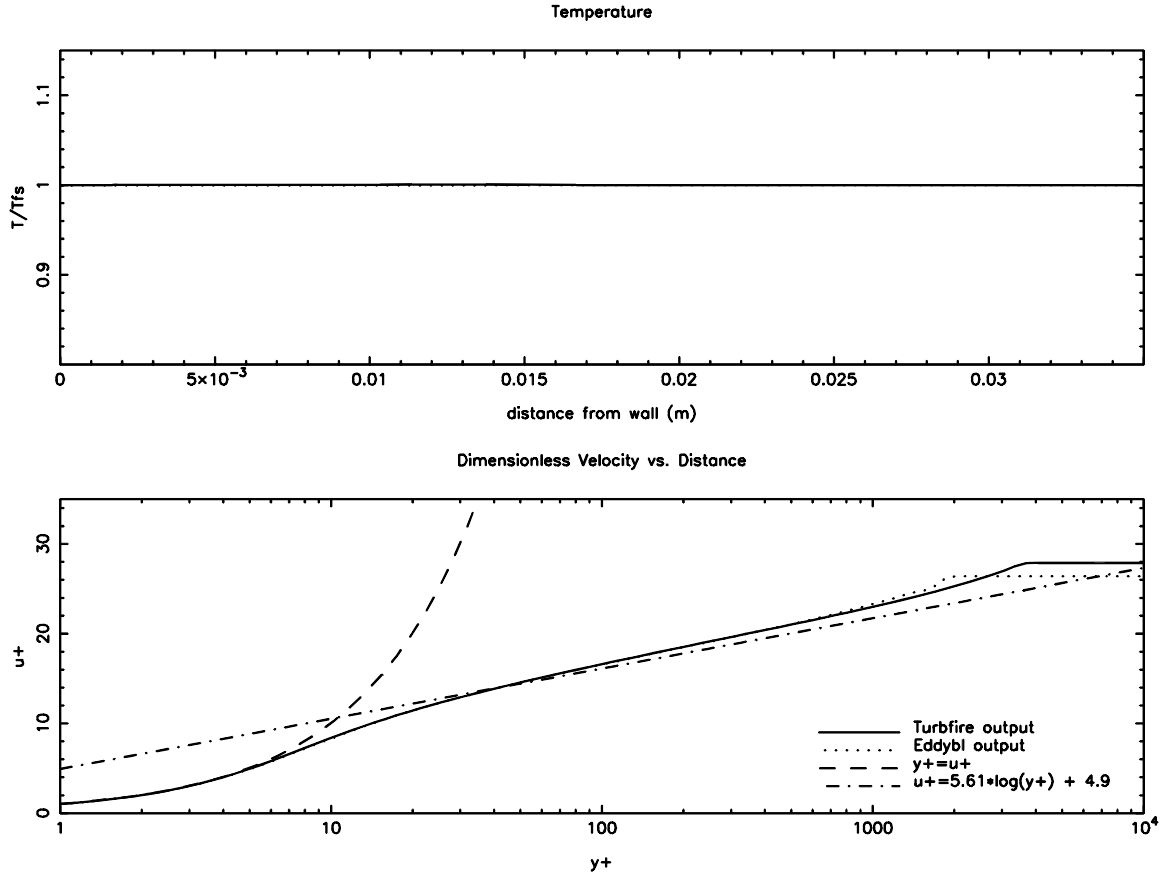

Figure 4.3 - Turbulent Benchmark Case 2: T_w=30000K, T_{fs}=30000K, P=500bar, $v_{x,fs}$=295m/s. (Ionization and radiation transport have been neglected for the purpose of comparing to EDDYBL results)

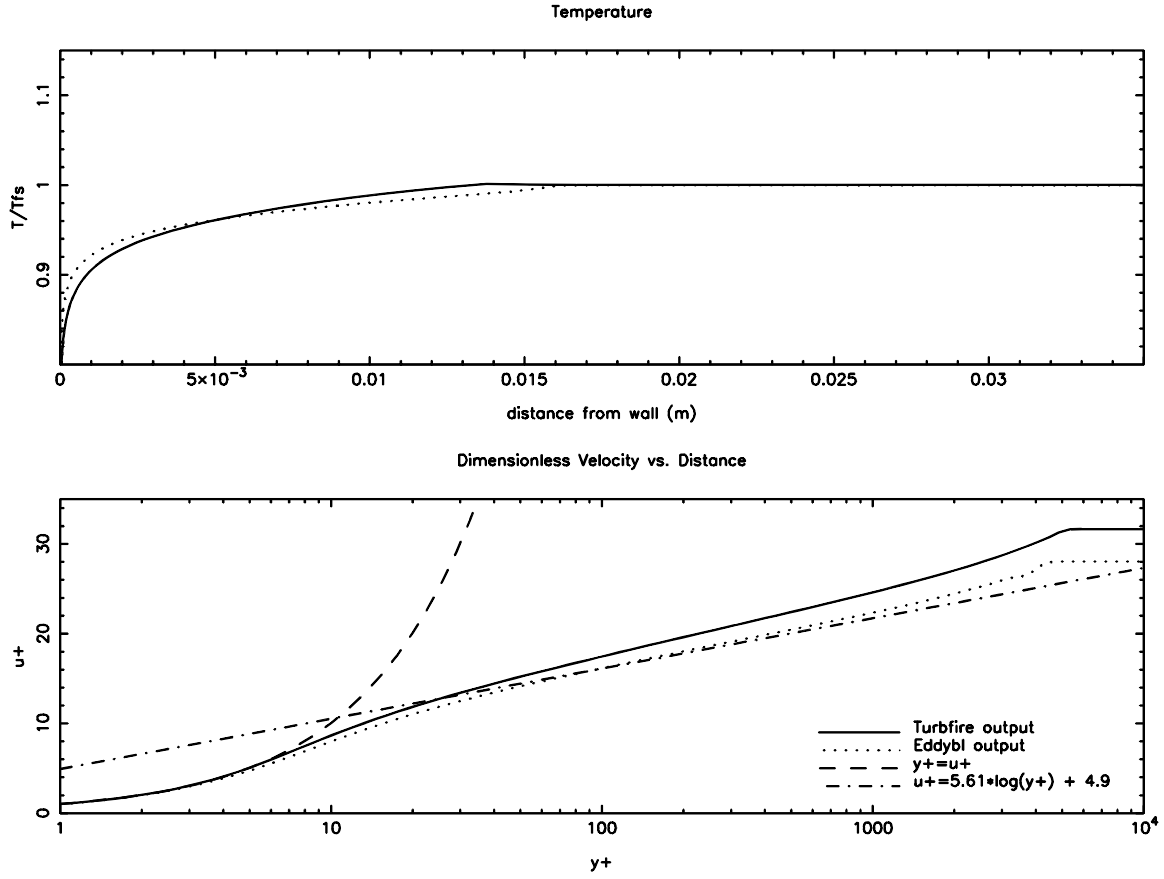

Figure 4.4 - Turbulent Benchmark Case 3: T_w=300K, T_{fs}=400K, P=1bar, $v_{x,fs}$=295m / s.

One aspect of the k-ω turbulence modeling that is different from its common usage is the application of boundary conditions at the free-stream. The k-ω model is typically used for flows for which free-stream values of k and ω are available from experimental data (flow measurements in pipes, wind tunnels, etc.), so these values can be used as boundary conditions. This type of data is not available for electrothermal plasma launchers or other plasma devices, so a zero-gradient boundary condition was used instead:

$$\frac{\partial k}{\partial y} = \frac{\partial \omega}{\partial y} = 0 \qquad (4\text{-}4)$$

TURBFIRE results were compared for runs with the zero-gradient boundary condition and with constant values of k_{fs} and ω_{fs}, for the flow of benchmark case 3 above. Results of this comparison are presented in Figure 4.5. Values for k_{fs} and ω_{fs} were obtained from the code run with zero-gradient boundary conditions. Since the free-stream values of k and ω change in the downstream direction, three runs were performed, using k_{fs} and ω_{fs} from: a) near the leading edge, b) the end of the run, and c) midway between the two. While using different values of k_{fs} and ω_{fs} caused slight differences in the velocity and temperature profiles, the temperature gradient near the surface was the same in all cases. This means that the conductive heat flux is not sensitive to the values chosen for k and ω at the free-stream.

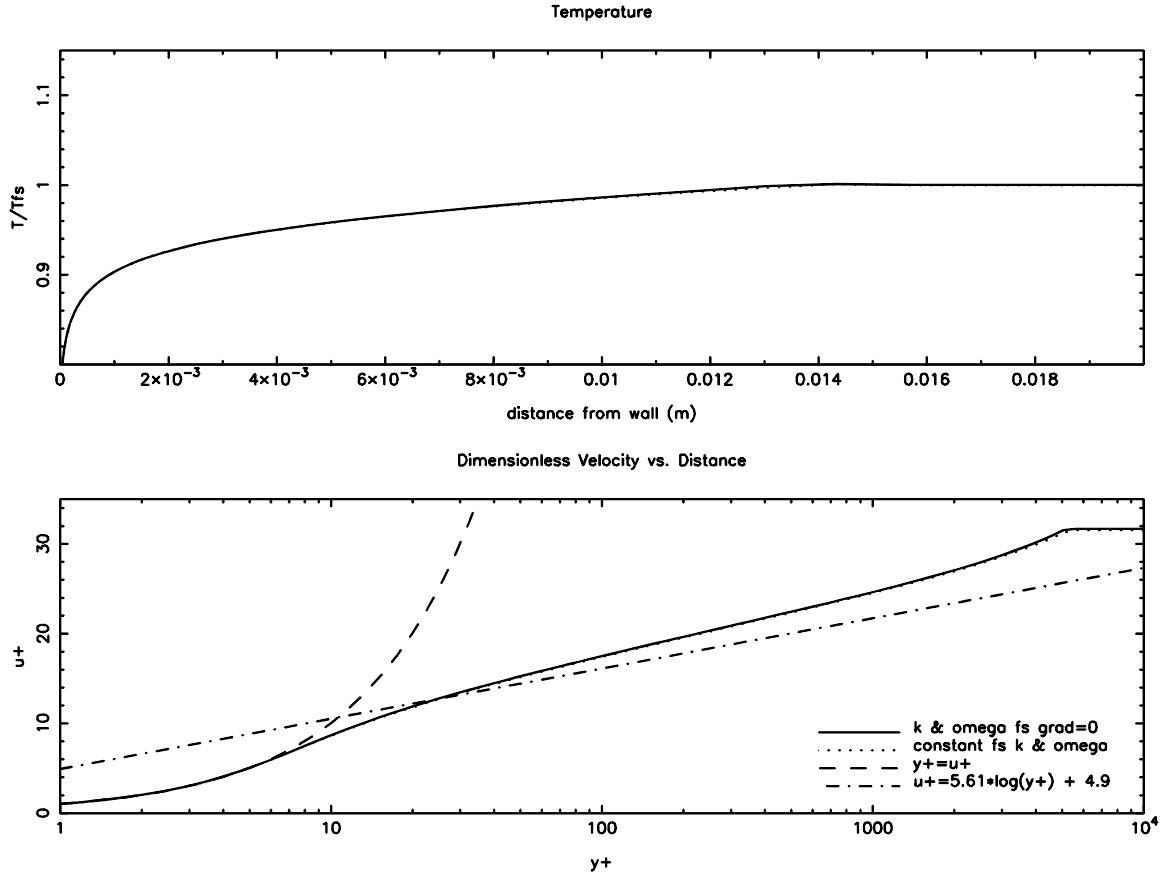

Figure 4.5 – Comparison of Turbulent Benchmark Case 3 results for constant vs. zero-gradient boundary conditions.

An important step in the development of the TURBFIRE code was the creation of a solution scheme that accounts for ionization and is stable for high temperatures. Conventional, low temperature flows are often modeled using an energy equation written in terms of temperature:

$$\bar{\rho}\tilde{v}_x C_P \frac{\partial \tilde{T}}{\partial x} + \bar{\rho}\tilde{v}_y C_P \frac{\partial \tilde{T}}{\partial y} = -\tilde{v}_x \frac{\partial P}{\partial x} + \mu\left(\frac{\partial \tilde{v}_x}{\partial y}\right)^2 + \beta^* \bar{\rho}\omega k + \frac{\partial}{\partial y}\left[\left(\lambda + \frac{C_P \mu_T}{Pr_T}\right)\frac{\partial \tilde{T}}{\partial y}\right] \qquad (4\text{-}5)$$

This energy equation can be used for gases or liquids because the heat capacity is only weakly dependent on temperature. For plasmas, however, the heat capacity varies significantly with temperature since it is dependent upon the charge state. This leads to stability problems when equation 4-5 is used to model even weakly ionized plasmas. Plots of heat capacity and average ionization state for different flows are presented in Figures 4.6 through 4.8. These results show that the heat capacity can vary by more than a factor of six over a very small range. TURBFIRE uses an energy equation written in terms of internal energy (equation 3.4), and temperature is calculated from equation 3.8.

Additionally, studies were done to test the importance of an accurate model for heat capacity. TURBFIRE was run using three models for C_v: 1) constant C_v; 2) C_v that varies linearly between its values at the wall and free-stream; and 3) $C_v = dU/dT$. Temperature profiles are presented in Figure 4.9 for each of these

models. Results of these changes show that using a fluid model for heat capacity will lead to an underestimate of the temperature gradient near the surface. This result illustrates the inadequacy of conventional gas models for fluid properties when modeling partially-ionized plasmas of relevance to electrothermal and electrothermal-chemical launch devices.

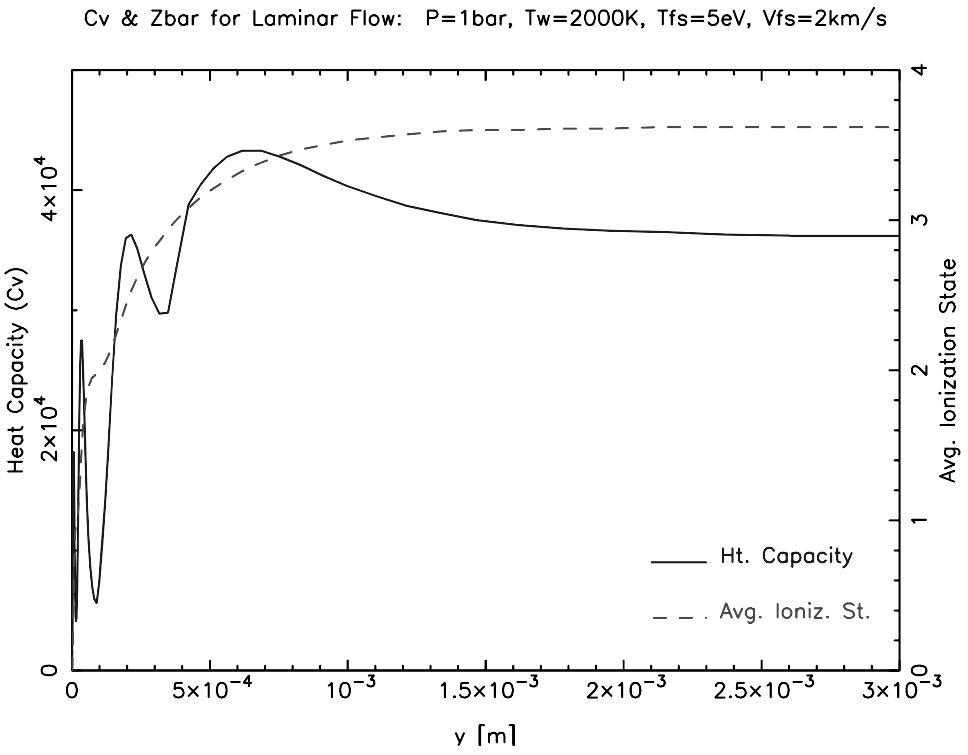

Figure 4.6 - Heat capacity and average ionization state for laminar flow with P=1bar

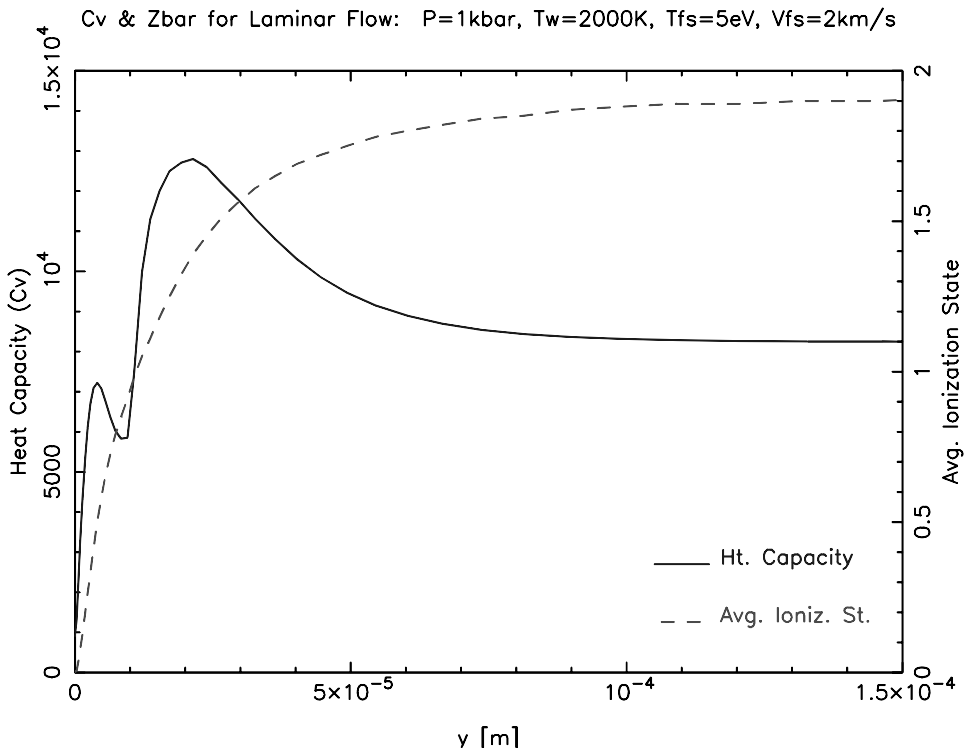

Figure 4.7 - Heat capacity and average ionization state for laminar flow with P=1kbar

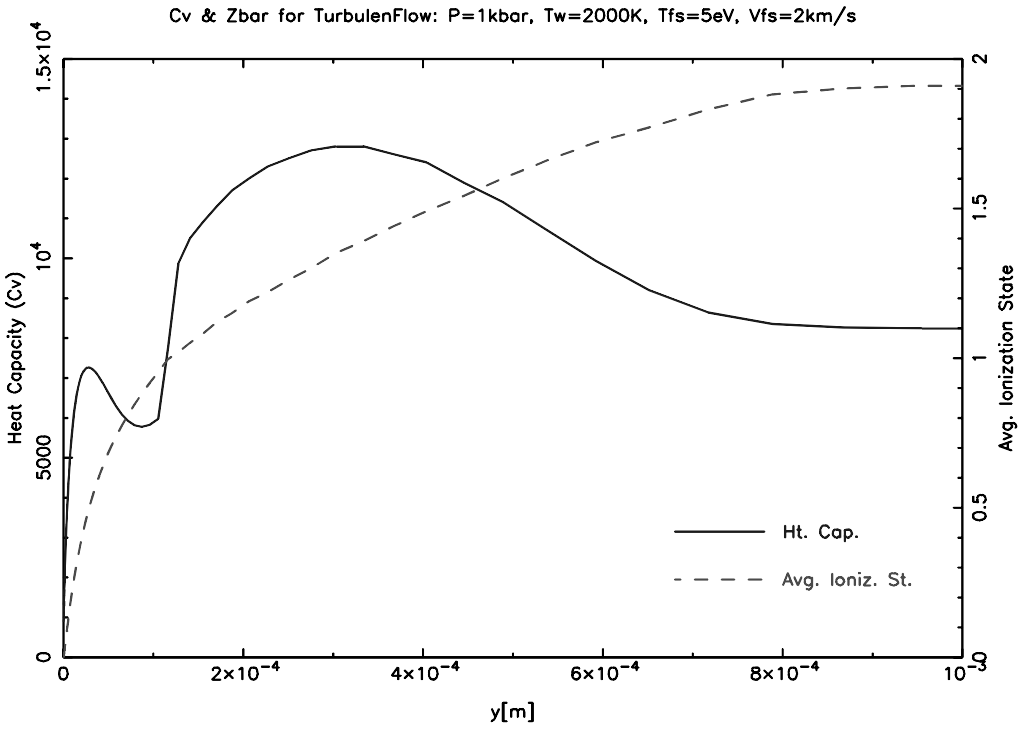

Figure 4.8 - Heat capacity and average ionization state for turbulent flow with P=1kbar

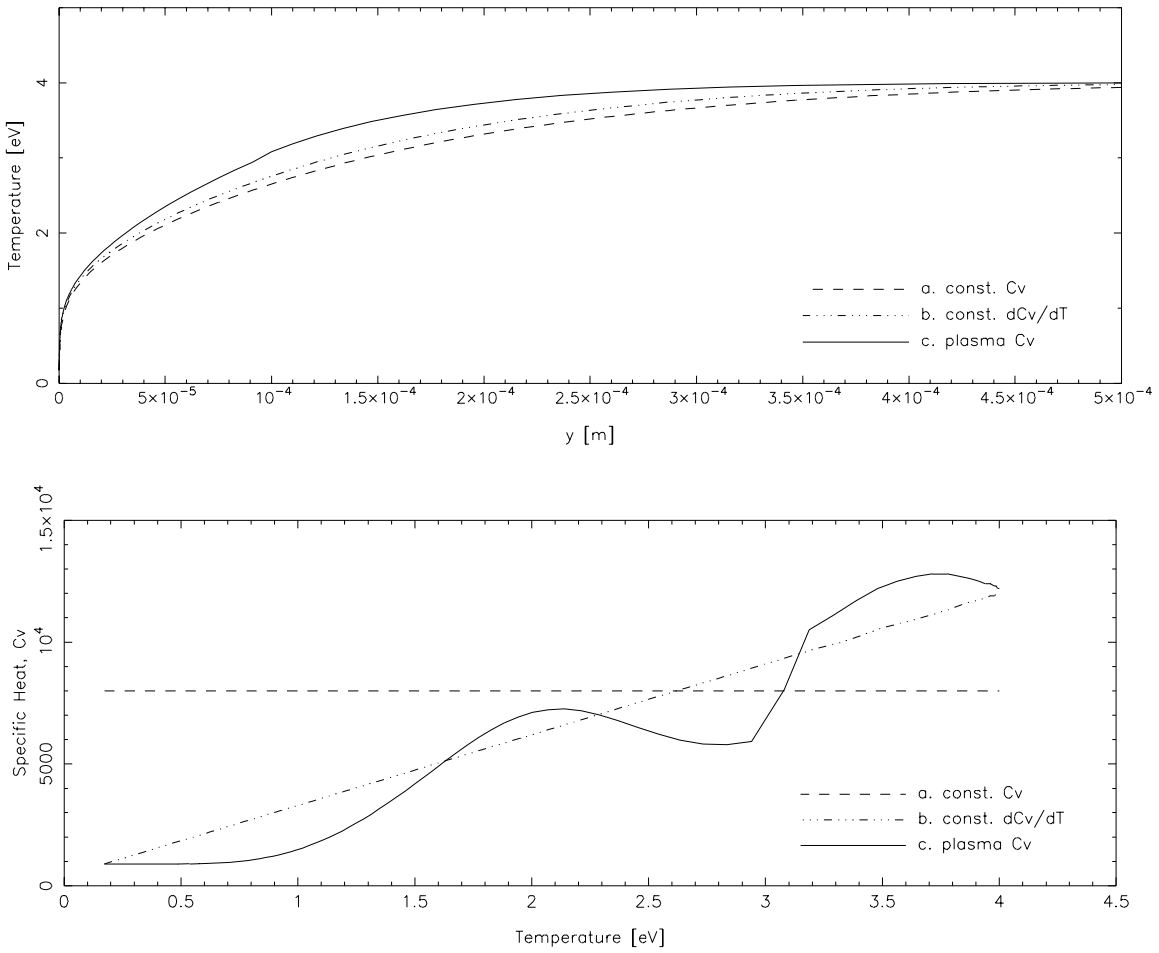

Figure 4.9 -A Comparison of Temperature Profiles Generated Using Three Models for C_V. P=1000bar, T_{wall}=2000K, T_{fs}=4eV, $v_{x,fs}$=1km/s

4.2 Test Cases with Radiation Transport

TURBFIRE results for runs with both turbulence and thermal radiation are presented in Figures 4.10 through 4.14. Code runs were done for iron and carbon plasmas as test cases with relevance to electrothermal launch devices, with T_w=5000K, T_{fs}=2.5eV, P=2kbar, $v_{x,fs}$=2km/s, and models of: 1) neither turbulence nor radiation; 2) turbulence but no radiation; 3) radiation but no turbulence; and 4) both turbulence and radiation. All results presented are at an axial distance of x=12cm, which is far enough downstream that the boundary layer is established and flow quantities such as temperature and velocity do not change significantly in the axial direction.

The results show that velocity and temperature gradients are larger near the wall with either radiation or turbulence (or both), and that the resulting boundary layers are wider. It is also evident that while only turbulence has a significant effect on the velocity profile, both radiation and turbulence cause a steeper temperature gradient near the wall. This indicates that models of both radiation transport and turbulence are important to accurately predict heat flux to the surface.

Results for both species show that the x-velocity is slightly higher for cases with radiation than without, and that the velocity profiles with radiation are slightly narrower. This is the case for both laminar and turbulent flow, for both species studied. The increased velocity is caused by slightly lower viscosity near the wall, which is the result of radiational heating of the near-wall plasma.

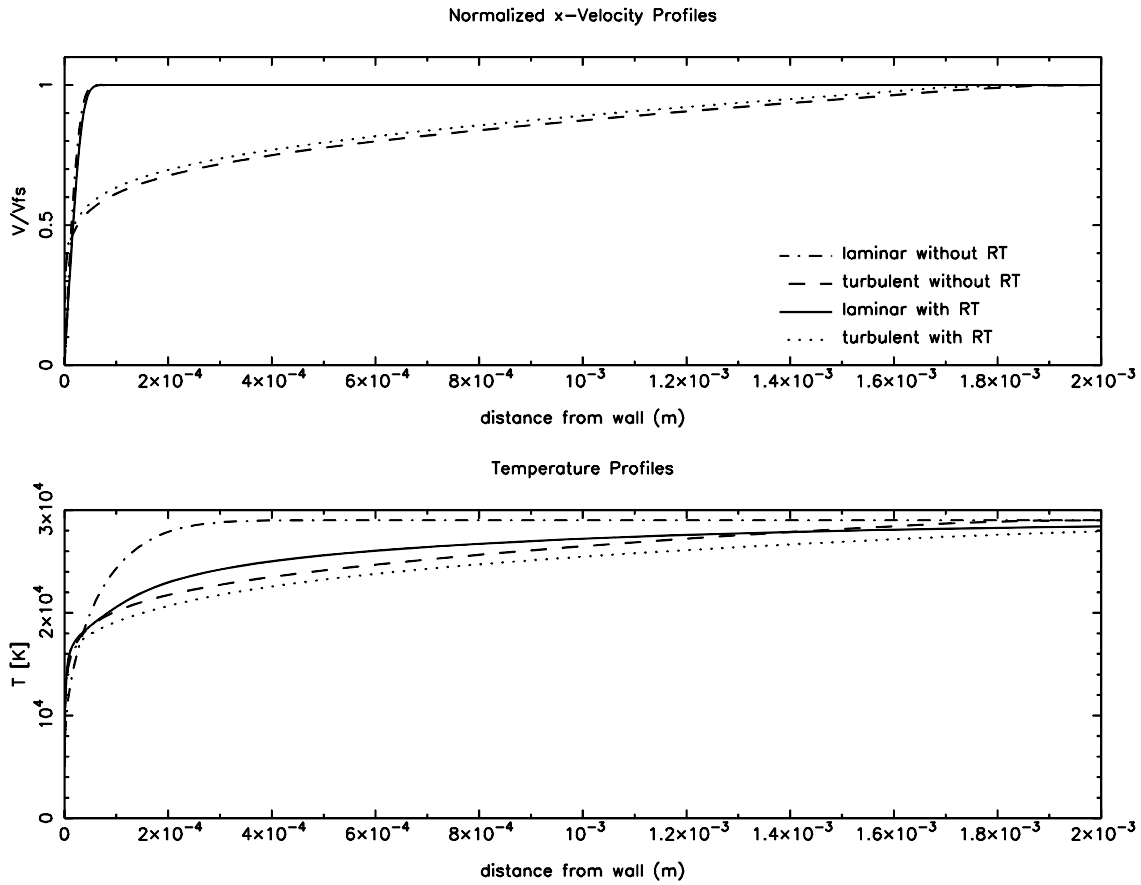

Figure 4.10 - Effects of Radiation and Turbulence on the Velocity and Temperature Profiles for an Iron plasma.
T_{fs}=2.5eV, T_{wall}=5000K, u_{fs}=2km/s, and P=2kbar

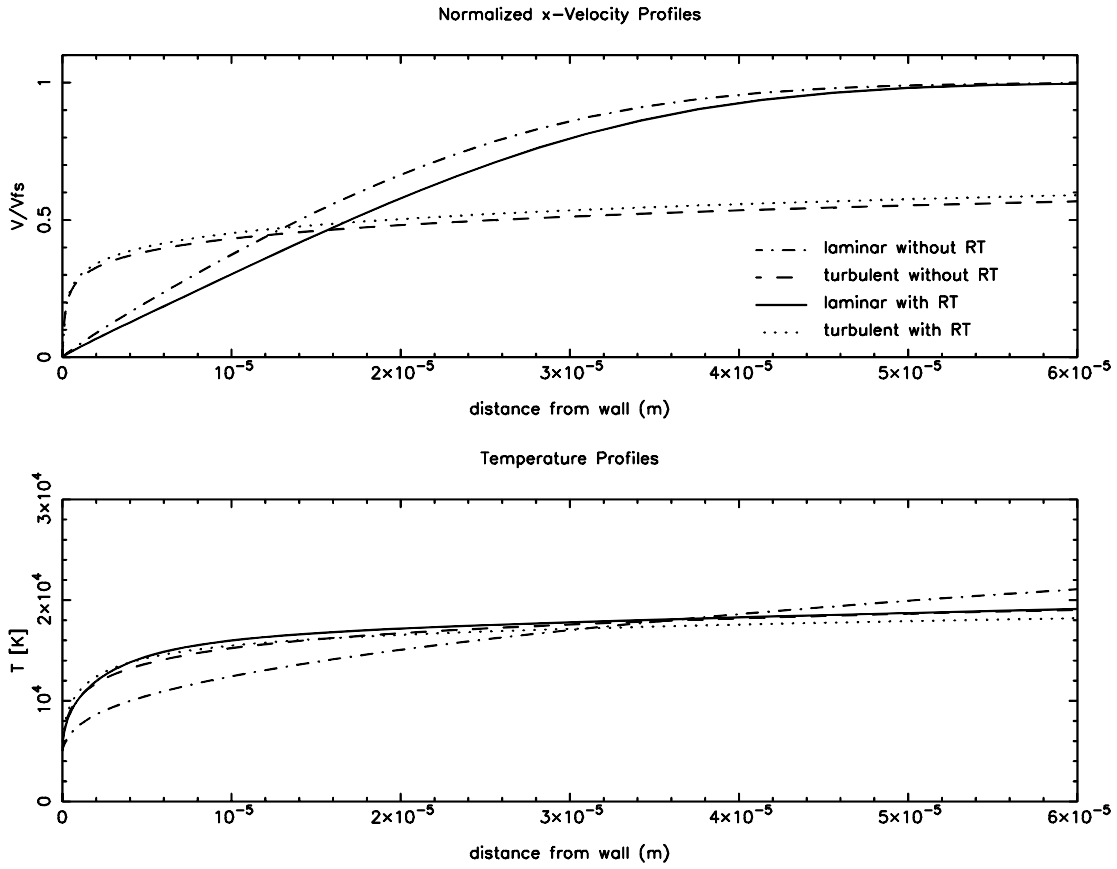

Figure 4.11 - Near-Wall Detail of Velocity and Temperature Profiles for an Iron plasma. T_{fs}= 2.5eV, T_{wall}= 5000K, u_{fs}=2km/s, and P=2kbar

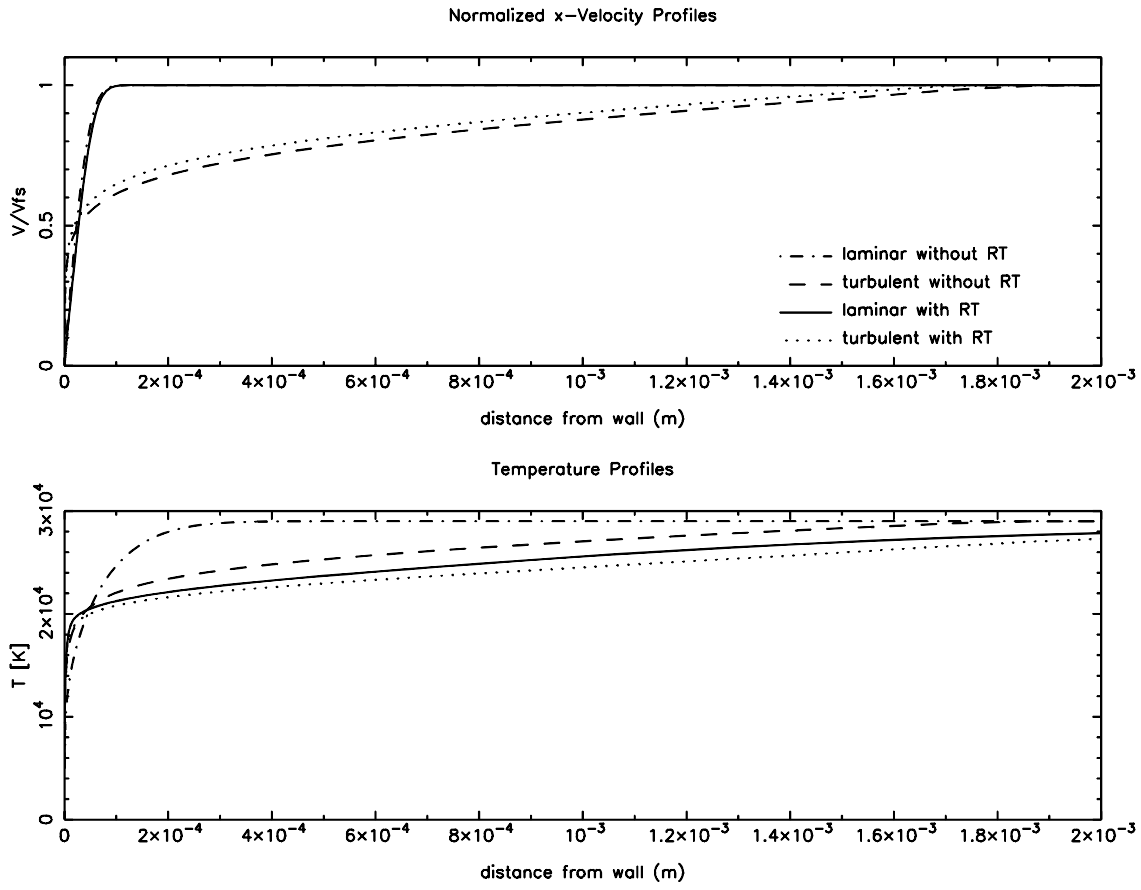

Figure 4.12 - Effects of Radiation and Turbulence on the Velocity and Temperature Profiles for a Carbon Plasma.
T_{fs}=2.5eV, T_{wall}=5000K, u_{fs}=2km/s, and P=2kbar

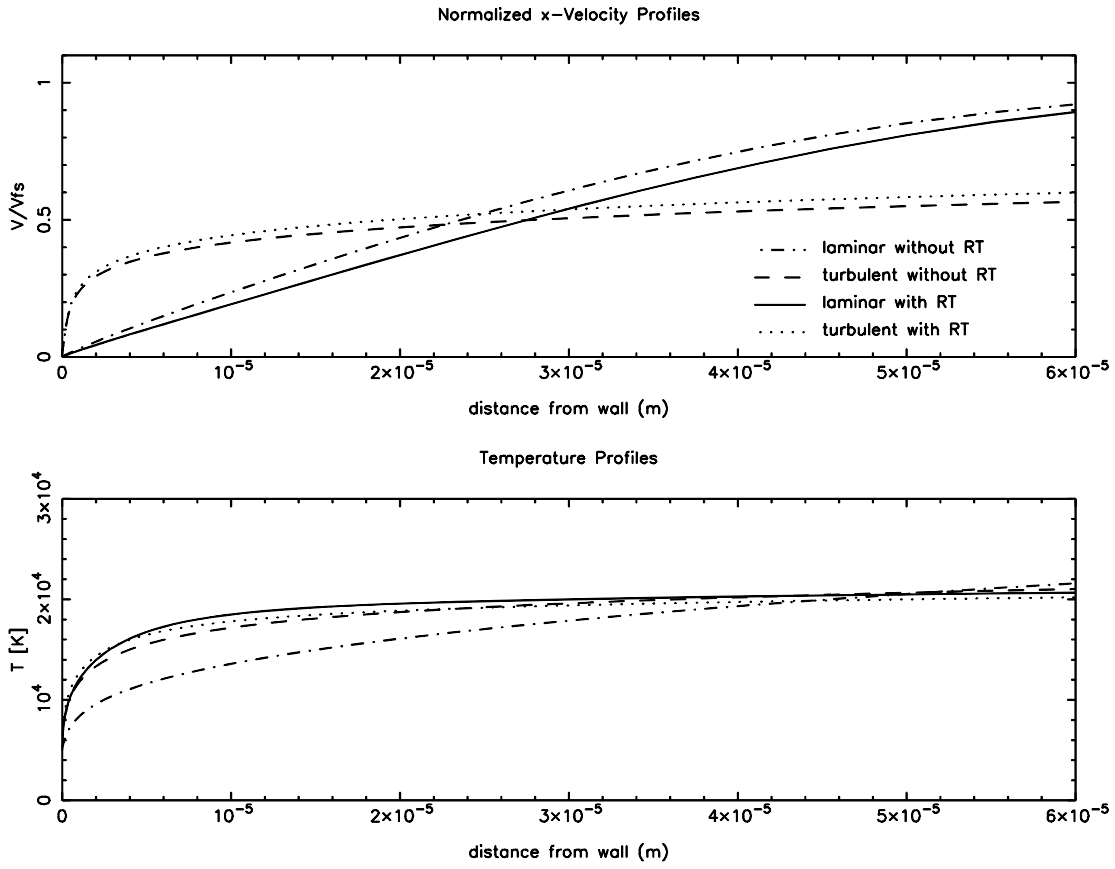

Figure 4.13 - Near-Wall Detail of Velocity and Temperature Profiles for a Carbon Plasma. T_{fs}=2.5eV, T_{wall}=5000K, u_{fs}=2km/s, and P=2kbar

Values of the heat flux to the wall for the code runs with iron and carbon are presented in Table 4.2. It is evident from these data that the combined effect of radiation and turbulence on the heat flux is less than the sum of their individual effects. Turbulence alone, for example, increases the wall heat flux by a factor of about 4.5 for an iron plasma, and radiation alone increases the heat flux by about a factor of 6. Together, however, they only cause an increase of about a factor of 8. This can be viewed as a mutual reduction of heating effectiveness by radiation and turbulence. It occurs because both turbulence and radiation decrease the temperature in most of the boundary layer, thereby increasing the amount of heat transport necessary (by radiation or turbulent convection) to further augment the heat flux to the wall. This effect can be seen clearly in the higher conductive heat flux for laminar flow with radiation, as compared to flow with radiation and turbulence.

While the code results show that both radiation and turbulence affect the temperature profiles for iron and carbon, the relative magnitude of their effects is different for each species. Turbulence appears to play about the same role for both species, increasing the radiative heat flux by about a factor of five. Radiation, however, has a larger effect for carbon than for iron. This is because the radiation mean free paths for iron are much shorter, so radiation from the hot free-stream plasma is more effectively shielded. The result is that the radiative heat flux to the surface for iron is only about a third as high as for carbon. The varying importance

of turbulence and radiation transport for different species further highlights the importance of including models of both phenomena.

Table 4.2 – Summary of the Heat Flux to the Surface via Conduction and Radiation (T_{fs}= 2.5eV, T_{wall}= 5000K, u_{fs}=2km/s, and P=2kbar)

Description	Heat flux [GW/m^2]					
	Iron			Carbon		
	q''_{cond}	q''_{rad}	q''_{tot}	q''_{cond}	q''_{rad}	q''_{tot}
Laminar, no radiation transport	0.88	-	0.88	0.76	-	0.76
Turbulent, no radiation transport	4.11	-	4.11	3.79	-	3.79
Laminar with radiation transport	3.46	2.00	5.46	3.77	6.60	10.37
Turbulent with radiation transport	5.06	1.85	6.91	4.85	6.15	11.00

It is also interesting to compare the conductive heat flux results for iron versus carbon. As discussed above, radiative heat fluxes are greater for carbon because of its longer radiation mean free paths. Conductive heat flux, however, is greater for iron in three of the four cases run, but greater for carbon in the other. This variation is caused by two competing factors. Near the wall, the thermal conductivity of the iron plasma is greater than for carbon, but in cases with radiation the temperature gradient is larger for carbon. Since conductive heat flux is given by:

$$q''_{cond} = k_{th} \frac{dT}{dy}$$

the two factors (thermal conductivity and temperature gradient) have opposite effects. In the cases without radiation, the heat flux is slightly greater for iron because of its higher thermal conductivity. With radiation alone, the near-wall temperature gradient for carbon is high enough to offset its lower thermal conductivity, so the conductive heat flux is higher than for iron. When the turbulence and radiation models are both included, however, the heat flux is greater for iron. This is because turbulence alone increases the near-wall temperature gradient nearly as much as turbulence and radiation combined, resulting in a temperature gradient for iron that is only slightly lower than for carbon.

4.3 Sensitivity Studies

As mentioned in the Method section, values commonly used for the turbulence model closure coefficients are not necessarily valid at the high temperatures and pressures present in electrothermal launchers. It would take a separate research project to fully investigate proper values for all of the coefficients used in the k-ω model, but it is especially important to investigate the effect of the turbulent Prandtl number, Pr_T. The turbulent Prandtl number is expected to have a significant effect on temperature profile because of its importance in the diffusion term of the energy equation (equation 3.4). A sensitivity study was performed to test whether the value chosen for Pr_T would affect the conclusion that both radiation transport and turbulence are important in modeling the boundary layer flow. In conventional fluid modeling a value of Pr_T=0.89 is generally used, so TURBFIRE was run for the same flow as in Figures 4.10 and 4.11 (iron plasma with T_{fs}=2.5eV, T_{wall}=5000K, u_{fs}=2km/s and P=2kbar), with the turbulent Prandtl number doubled and halved (Pr_T=0.445 and 1.78). The results of these runs are presented in Figure 4-14.

Since the turbulent Prandtl number appears in the denominator of the diffusion term, a larger Pr_T is expected to reduce turbulent convection and decrease turbulent energy transport to the surface. This effect is apparent in the temperature profiles in Figure 4.14, which are wider and steeper near the wall for code runs with Pr_T halved and less steep with Pr_T doubled. In all three cases, however, the

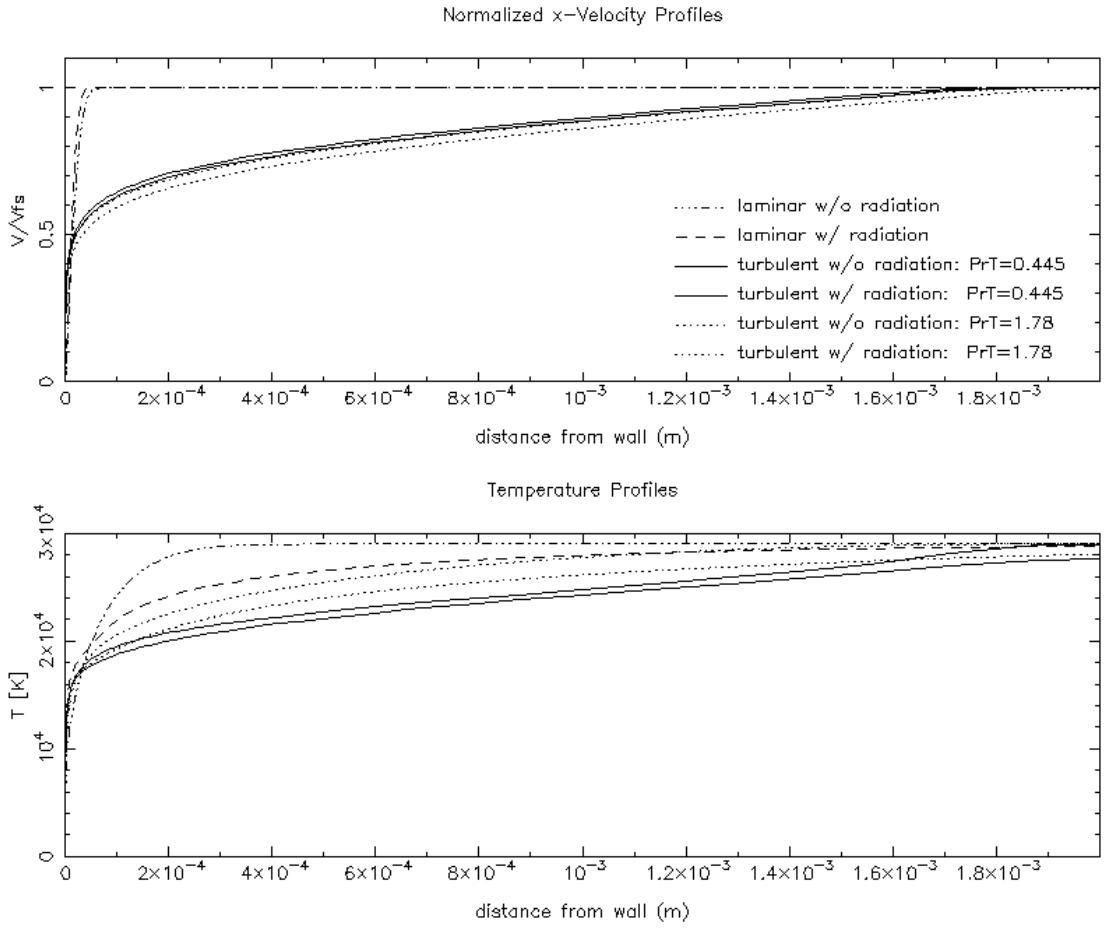

Figure 4.14 - Sensitivity study to determine the effect of varying Pr_T on temperature and velocity profiles (iron plasma with T_{fs}=2.5eV, T_{wall}=5000K, u_{fs}=2km/s, and P=2kbar). For each value of Pr_T, the run with radiation transport corresponds to the slightly narrower velocity profile and slightly wider temperature profile.

addition of the radiation transport model increases the temperature gradient near the wall, so both turbulence and radiation are important regardless of the value chosen for Pr_T.

A sensitivity study was also carried out to determine the importance of the near-wall thermal conductivity model on the results. In most of the boundary layer, the average ionization state is high enough that free electrons are the main carriers of thermal energy. Where this is the case, a plasma model (equation 3-14) for thermal conductivity is appropriate. For some flows, however, the ionization state near the wall may be low enough that a fluid model (Table 3.2) of thermal conductivity is necessary. The TURBFIRE code calculates thermal conductivity near the wall using both plasma and fluid models, and the greater of the two is chosen. No fluid model was available for thermal conductivity at the high temperatures and pressures present near the wall of an electrothermal launcher (T≈5000K, P≈1kbar), so available fluid models were extended to higher temperature and pressure. To investigate whether the use of these models would have an effect on the results, TURBFIRE was run with the thermal conductivity from the fluid model doubled. For the code runs presented in Section 4.2, the thermal conductivity from the plasma model was greater than that from the fluid model all the way to the wall, so the code used only the plasma model. With the fluid-model thermal conductivity doubled, however, it is greater than that from the plasma model at the first few mesh points nearest the wall. Because it is used in only a

very small part of the boundary layer, doubling the fluid-model thermal conductivity does not effect temperature profiles enough to be seen in a plot. The maximum difference in Temperature between the three cases is about 2% near the wall.

Table 4.3 presents wall heat fluxes for the sensitivity studies on both turbulent Prandtl number and wall heat flux. As discussed above, a larger Pr_T decreases turbulent energy transport to the surface, since Pr_T appears in the denominator of the diffusion term. The choice of Pr_T has only a small effect on the radiative energy flux to the wall. Absorption and emission of radiation are not changed much by the small differences in temperature profiles caused by different values of Pr_T. In general, cases with a narrower boundary layer have a higher radiative energy flux, but even the largest difference (between the case with Pr_T=.445 and that with the turbulence model turned off) is small compared to the change in conduction.

The effect of doubling the near-wall thermal conductivity is an increased heat flux to the wall via conduction. The temperature at the mesh point nearest the wall is slightly lower in these cases due to the increased conductivity, so the conductive flux is not doubled. Radiation flux is essentially unaffected, since the temperature away from the wall is not significantly changed.

Table 4.3 – Summary of the Heat Flux to the Surface for Sensitivity Studies (iron plasma with T_{fs}=2.5eV, T_{wall}=5000K, u_{fs}=2km/s, and P=2kbar)

Description	Heat flux [GW/m^2]											
	Pr_T						Fluid-model thermal conductivity					
	0.445		0.89		1.78		$K_{th,fl}/2$		$K_{th,fl}$		$2*K_{th,fl}$	
	q''_{tot}	q''_{rad}	q''_{tot}	q''_{rad}	q''_{tot}	q''_{rad}	q''_{tot}	q''_{rad}	q''_{tot}	q''_{rad}	q''_{tot}	q''_{rad}
Laminar, no radiation transport	0.88	-	0.88	-	0.88	-	0.88	-	0.88	-	0.91	-
Turbulent, no radiation transport	5.75	-	4.11	-	2.89	-	4.11	-	4.11	-	4.87	-
Laminar with radiation transport	5.46	2.00	5.46	2.00	5.46	2.00	5.46	2.00	5.46	2.00	5.99	2.00
Turbulent with radiation transport	8.24	1.84	6.91	1.85	6.03	1.87	6.91	1.85	6.91	1.85	8.07	1.85

It is important to note that the values of both Pr_T and near-wall thermal conductivity do affect the heat flux to the wall. The heat flux values presented in Tables 4.2 and 4.3 should therefore be taken as an illustration of the relative contributions of radiation and turbulence, rather than a prediction of the precise values of heat flux that would be measured in an experiment. Regardless of the values of these quantities, however, it can be concluded that both turbulence and radiation transport are important mechanisms of energy transport to the surface.

4.4 Test Cases with Ablation

Simple models of ablation and near-wall physics were included in the model to allow the investigation of vapor shielding and the effects of ablation on the results of the previous sections. TURBFIRE results for runs with ablation are presented in Figures 4.15 through 4.18. Code runs were done with iron as both the bulk plasma and the ablated wall material, with T_w=9710K, T_{fs}=2.5eV, P=2kbar, $v_{x,fs}$=2km/s.

When running the code with ablation, care had to be taken to choose cases in which the flow would not separate. As heat flux to the surface increases, the amount of ablated material shows a corresponding increase. In much the same way as for conventional fluid flow with blowing, separation can occur if the rate at which material leaves the surface becomes too high. Since the TURBFIRE code uses a forward-marching solution scheme, it cannot model cases in which the flow separates. To keep heat flux to the wall low enough to avoid separation, TURBFIRE runs with ablation have wall and free-stream temperatures that are closer together than might be expected in many electrothermal plasma devices. It is suggested that future codes (or further modifications of TURBFIRE) implement a solution scheme that can model separating flow. This was not practical for the current version of TURBFIRE because it would require either modeling of less physics or prohibitively long run times. Despite this limitation, however, TURBFIRE can provide insight into the effects of ablation on energy transport to the surface.

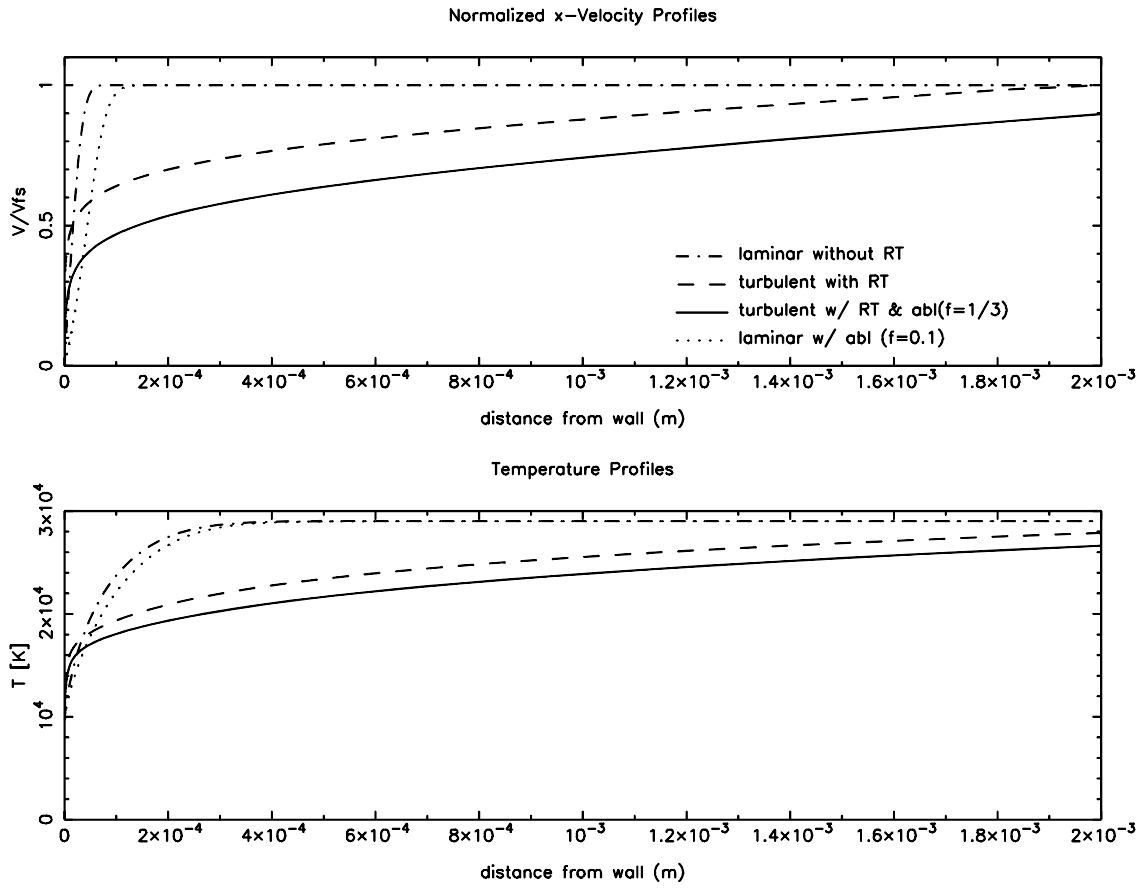

Figure 4.15 - Effects of Ablation on the Velocity and Temperature Profiles for an Iron plasma. T_{fs}=2.5eV, T_{wall}=9710K, u_{fs}=2km/s, and P=2kbar

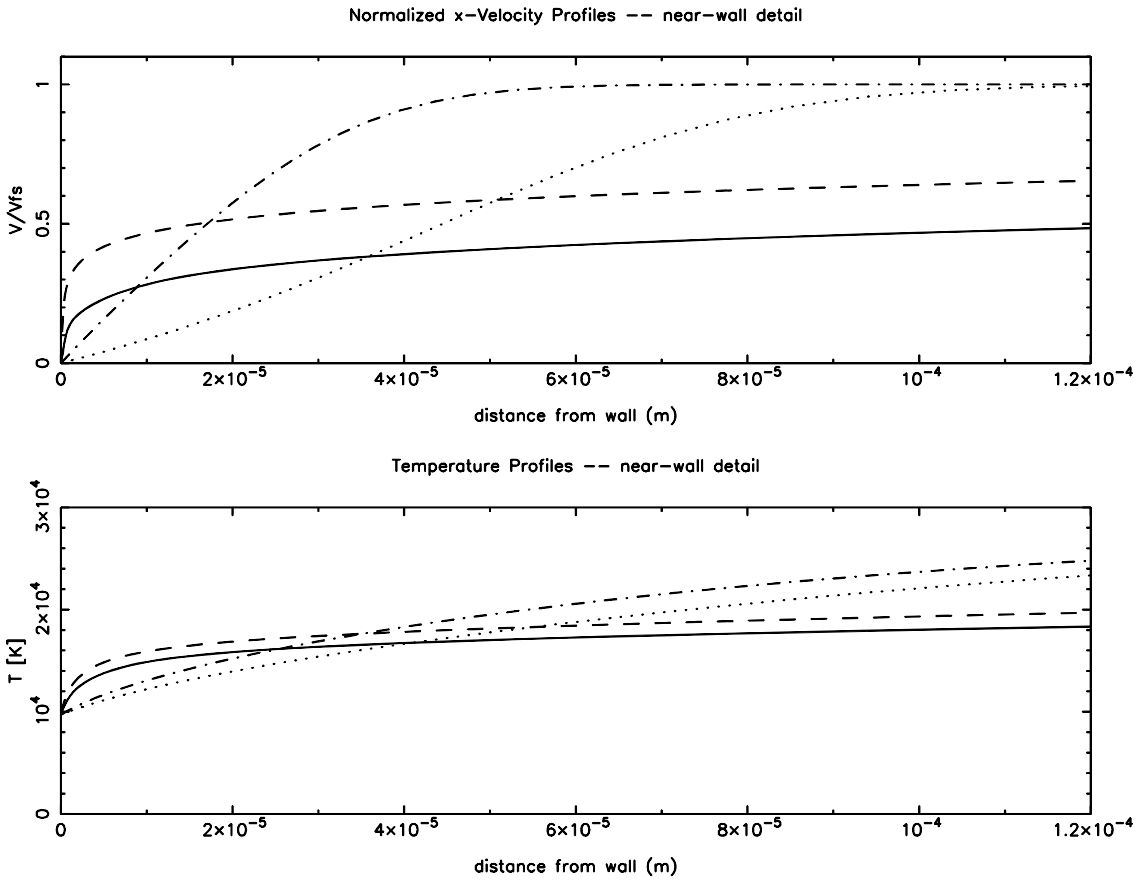

Figure 4.16 - Near-Wall Detail of Velocity and Temperature Profiles for an Iron plasma with ablation. T_{fs}=2.5eV, T_{wall}=9710K, u_{fs}=2km/s, and P=2kbar

In order to run cases with free-stream temperatures high enough for radiation transport, code runs with ablation were done with a wall temperature equal to the saturation temperature at a pressure of 2kbar. For Iron, $T_w=T_{sat}=9710K$, from the equation:

$$\log P_{sat} = -19710.0/T_{sat} - 1.27\log T_{sat} + 13.27 \qquad (4\text{-}6)$$

Results for runs with ablation show that temperature and velocity profiles near the wall are wider with ablation than without, and that ablation reduces the near-wall gradients of both. In this way, ablation is analogous to the case of conventional fluid flow with blowing. As with the cases without ablation (section 4.2), the results show that both turbulent convection and radiation transport play important roles in energy transport to the surface.

As discussed in the Method section, f_{abl} is the fraction of energy incident on the wall that goes into ablating surface material. Since much of the incident energy is conducted into the wall, the fraction of energy that causes ablation must satisfy the relation $0<f_{abl}<1$. Depending on the wall material, incident energy can also be lost (at least locally) to phase changes. The TURBFIRE code does not currently include a model for wall conduction, so values of $f_{abl} = 1/3$ and 0.1 have been used for the present study. While f_{abl} may be higher or lower in some plasma devices, the values used are sufficient to satisfy the goals of this research, which are to

investigate the effects of ablation, turbulence and radiation on energy transport in the boundary layer.

For the laminar case, the code could not be run with $f_{abl}=1/3$ because the flow separated. This did not happen for turbulent flow because of turbulent mixing, which brings higher velocity fluid closer to the wall. Results of runs to a shorter distance are presented in Figure 4.17. This shorter distance is less than the distance to separation, so the laminar case could be run. The results further demonstrate the self-limiting nature of ablation, since increasing the amount of ablation reduces velocity and temperature near the wall. The cases presented in Figure 4.17 were not run far enough downstream to be considered converged solutions, so values of the heat flux to the wall are not presented. It should be noted that while the laminar case is not physically reasonable, it provides a base case from which the effects of radiation, turbulence and ablation can be analyzed.

A summary of heat flux to the wall for cases with ablation is presented in Table 4.3. The results show that for both laminar and turbulent flow there is a hydrodynamic vapor shielding effect even in the case where radiation transport is neglected. This can be attributed to the more gradual temperature gradient near the wall, caused by the outward motion of relatively cool ablated material. It is evident from the heat flux as well that both turbulence and radiation play a significant role in energy transport in the boundary layer. While ablation reduces

the heat flux to the wall for all cases modeled, the wall heat flux is still greatest for the cases run with both radiation and turbulence.

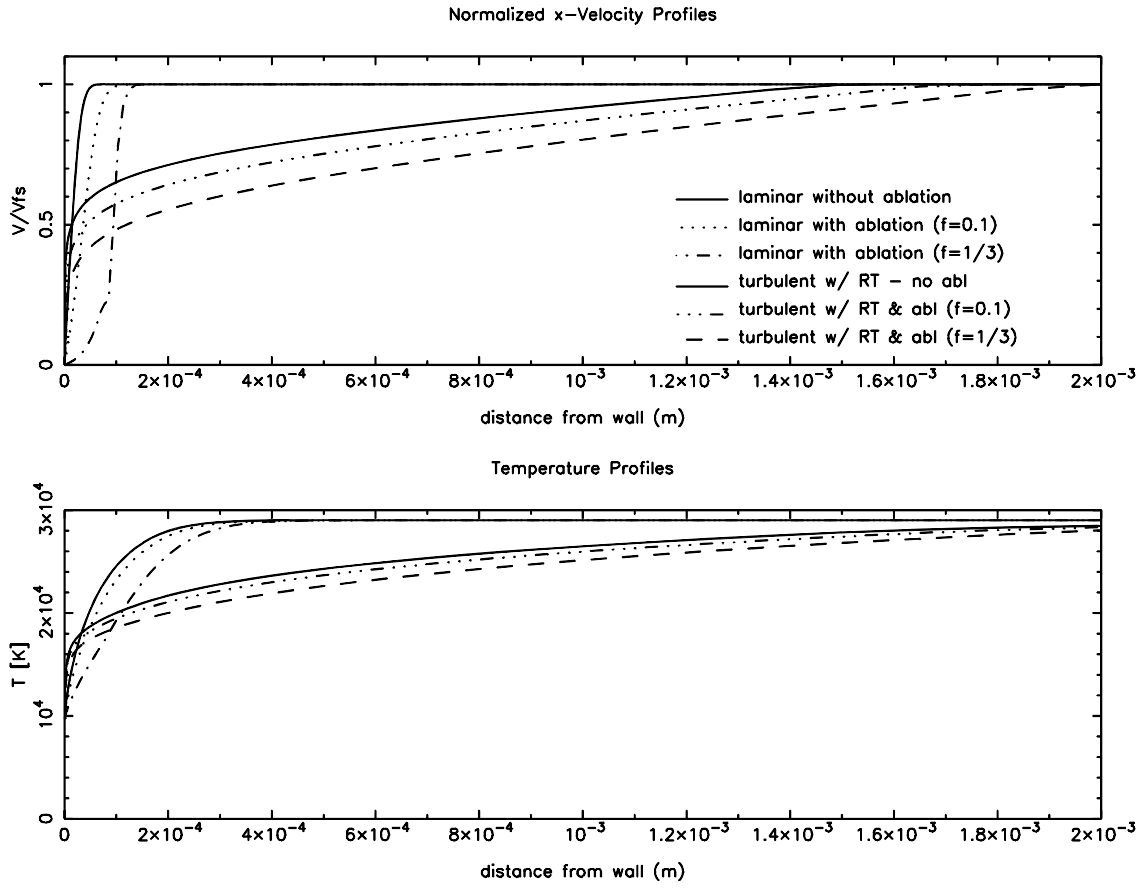

Figure 4.17 - Effects of different values of f_{abl} on the Velocity and Temperature Profiles for an Iron plasma.
T_{fs}=2.5eV, T_{wall}=9710K, u_{fs}=2kms, and P=2kbar

Table 4.4 - Summary of the Heat Flux to the Surface for Cases with Ablation (Iron plasma. T_{fs}=2.5eV, T_{wall}=9710K, u_{fs}=2km/s, and P=2kbar)

Description	Heat flux [GW/m^2]								
	no ablation			ablation with f_{abl}=0.1			ablation with f_{abl}=1/3		
	q''_{cond}	q''_{rad}	q''_{tot}	q''_{cond}	q''_{rad}	q''_{tot}	q''_{cond}	q''_{rad}	q''_{tot}
Laminar, no radiation transport	0.79	-	0.79	0.54	-	0.54	-	-	-
Turbulent, no radiation transport	4.55	-	4.55	3.95	-	3.95	3.17	-	3.17
Turbulent with radiation transport	6.19	2.17	8.36	5.13	2.07	7.20	3.65	1.86	5.51

The energy transmission fraction, defined as the ratio of the energy reaching the wall to the total energy emitted towards the wall by the free-stream plasma, can be written:

$$f_{tr} = \frac{q''_w}{q''_{fs}} = \frac{q''_w}{\sigma T^4} \tag{4-7}$$

where q''_{fs} and q''_w are both in the negative-y direction (towards the wall). For the code runs presented, T_w=2.5eV, so $q''_{fs} = \sigma T^4 = 40.2\,GW/m^2$. Values of the transmission fraction are presented in Table 4-4.

It is important to note that at the high temperatures and velocities present in electrothermal launchers, flow is highly turbulent and radiation transport is

Table 4.5 - Summary of the Transmission Fraction for TURBFIRE Runs with Varying Amounts of Ablation
(Iron plasma. T_{fs}=2.5eV, T_{wall}=9710K, u_{fs}=2km/s, and P=2kbar)

Description	**f_{tr}**		
	no ablation	**ablation: f_{abl}=0.1**	**ablation: f_{abl}=1/3**
Laminar, no radiation transport	0.020	0.013	-
Turbulent, no radiation transport	0.113	0.098	0.079
Turbulent w/ radiation transport	0.208	0.179	0. 137

important. Results for laminar flow and turbulent flow without radiation are presented for the sake of analysis, but only the results with both turbulence and radiation are physically reasonable. Results for all cases illustrate a hydrodynamic vapor shielding effect, which is evident for both laminar and turbulent flow. It is unclear from the present study how much of the shielding seen in the cases with both radiation and turbulence is due to these hydrodynamic effects. An interesting future project would be to further investigate the mechanisms of vapor shielding, to try and determine the relative effects of hydrodynamic versus radiation transport effects.

Because TURBFIRE is a steady-state code, results cannot be directly compared with experimental results from the SIRENS electrothermal launcher experiment. It is encouraging to note that the results match transmission fractions

of f_{tr}=5-20% reported in the literature by Hahn[10] from the MAGFIRE code, Bourham et al.[1] for SIRENS, and Kovitya and Lowke[17].

As discussed in the Method section, it is possible to test whether the plasma meets the criteria for local thermodynamic equilibrium (LTE) and the diffusion approximation. For the plasma to be considered at LTE, the electron density and temperature must satisfy the relation[29]: $n_e > 10^{22} T_{eV}^{7/2}$ [m^{-3}]. The right-hand-side of this expression is plotted in Figure 4.18, along with the electron density from the TURBFIRE code. It is clear from the graph that the dense electrothermal gun plasmas being modeled meet this LTE criterion. This is in agreement with the findings of Murali[23] and Ngo[25], who showed that plasmas in electrothermal launchers such as SIRENS are at LTE. To investigate the validity of the diffusion approximation, mean free paths were calculated. For all runs with ablation, the radiation mean free paths were found to be smaller than the mesh dimensions.

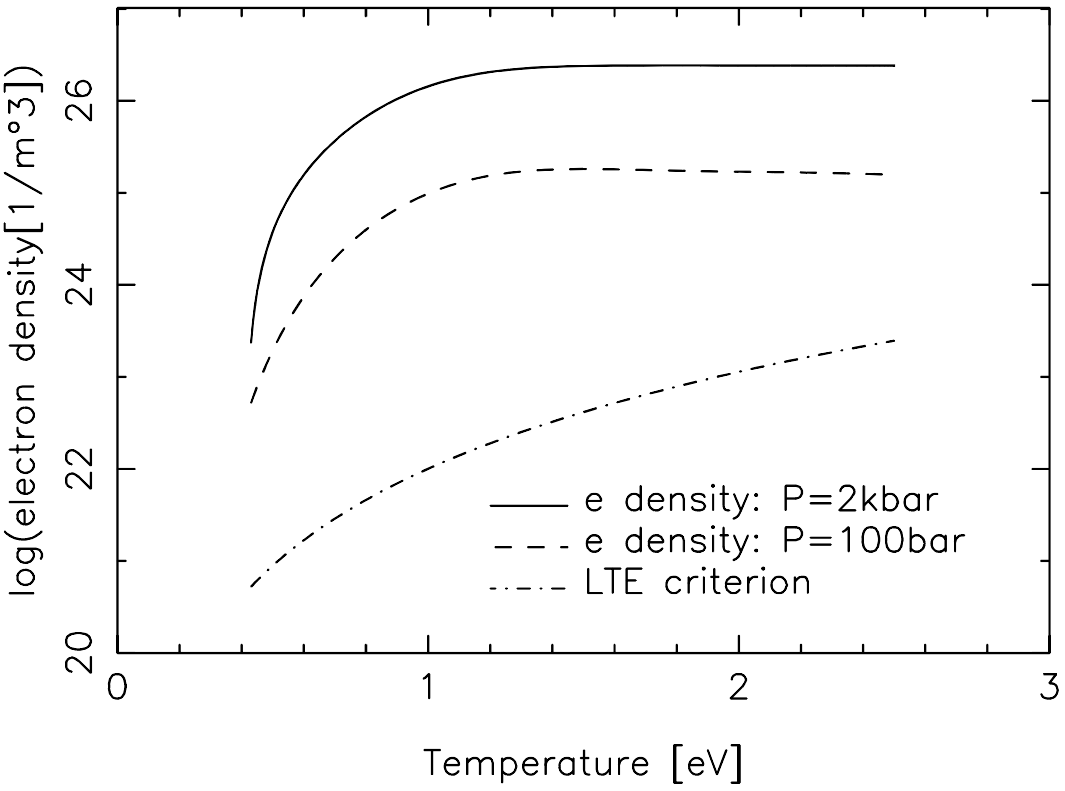

Figure 4.18 - Turbfire electron density for an electrothermal launcher plasma T_{fs}=2.5eV, T_{wall}=9710K and u_{fs}=2 km/s

5. CONCLUSIONS AND RECOMMENDATIONS

The purpose of this research was to develop a model of boundary-layer energy transport in electric launchers, and perform a numerical simulation to investigate the influence of turbulence, thermal radiation and ablation on energy flux to the surface. The model developed combines boundary-layer conservation equations with a k-ω turbulence model and multi-group radiation transport, and uses plasma models for fluid properties such as viscosity, thermal conductivity and specific heat capacity. The resulting TURBFIRE computer code is the first code to model turbulence, radiation transport and ablation in a self-consistent manner for plasma flow along a surface

TURBFIRE results for conventional low-temperature flows were compared to results from the EDDYBL code[31]. These benchmark cases demonstrate that the model in TURBFIRE accurately predicts laminar and turbulent flow on a flat plate. Some concerns over use of the code to measure higher temperature flows were addressed in sensitivity studies of the turbulent Prandtl number and the near-wall thermal conductivity, but further work in this area is recommended. Specifically, an investigation of the proper values for turbulence model closure coefficients would make the code more useful for predicting precise values of wall heat flux. Also, the addition of time dependence to TURBFIRE would allow direct comparison of the results to measured data from electrothermal launchers and other relevant experiments. Time dependence has not been included in the current

version of TURBFIRE because of the long run time already required for the steady-state solution.

One new aspect of the turbulence model used in this research is the adoption of zero-gradient boundary conditions for k and ω at the free-stream. In conventional flow modeling, experimental data is generally used to provide values of k and ω at the free-stream. This type of data is not available for electrothermal launchers, so test cases were run to determine whether a zero-gradient boundary condition could be used instead. Results of these runs showed that the temperature and velocity profiles generated by TURBFIRE were essentially identical with the two sets of boundary conditions.

TURBFIRE was run with both radiation and turbulence under electrothermal launcher conditions (P=2kbar, T_{fs}=2.5eV, $v_{x,fs}$=2km/s). In order to evaluate the influence of radiation and turbulence on energy flux to the surface, the code was run for both iron and carbon plasmas. Results show that both phenomena increase the heat flux to the surface, and that their combined effect is not additive. This was found to be true regardless of the plasma species or the values of parameters investigated in the sensitivity studies. This result indicates that both radiation transport and turbulence must be included in any model of boundary-layer energy transport in electric launch plasma devices.

A comparison of results for iron and carbon reveals that while the effect of turbulence doesn't change much for different species, the effect of radiation is

strongly dependent on properties of the plasma species, such as thermal conductivity and absorption and emission coefficients. Values of heat flux via radiation and conduction also changed significantly due to changes in these properties. In all cases, however, both turbulence and radiation transport were found to be important, and conductive and radiative flux were both significant. This last result contradicts previous research by Hahn et al.[9,10] who found that the conductive flux to the wall was negligible. This contradiction is likely due to the differences in the models used. Hahn's 1-D, time-dependent MAGFIRE code did not model flow in the direction parallel to the wall, nor did it include a model of turbulence. Results of the present research show that without a turbulence model, the radiation flux to the wall is overestimated, while the conduction flux is underestimated. Additionally, the MAGFIRE code modeled pressure-driven expansion of ablated material away from the wall, so the ablated material velocity was higher and the near-wall temperature gradient smaller than with the model in TURBFIRE. If time dependence and compressibility are added to TURBFIRE, the results could be directly compared to those from MAGFIRE, and the effects of turbulence and the 2-D flow model could be more thoroughly investigated. Other studies[15,17,24] have also concluded that conduction is negligible. Based on the results of this research, it is important draw a distinction between the bulk, free stream plasma, where that is probably true, and the boundary layer, where it is not.

TURBFIRE was run with ablation to investigate vapor shielding and the importance of radiation transport and turbulence in ablative flows. Results confirm the finding of Eapen[4], that there is a purely hydrodynamic shielding effect even without the inclusion of radiation transport. An interesting topic for future research would be to investigate the mechanisms of this shielding to determine how much of the shielding seen with radiation transport is caused by absorption and re-distribution of radiation energy, and how much is the result of hydrodynamic phenomena.

Results with ablation, turbulence and radiation transport together support the conclusion that both turbulence and radiation are important mechanisms of energy transport to the surface. The effects of radiation and turbulence were qualitatively the same for cases with ablation as for cases without. Both increased heat flux to the surface and widened the boundary layer. The main effect of ablation was to "push" the temperature and velocity profiles away from the wall, thereby reducing the heat flux. The energy transmission fractions for cases run with turbulence, radiation transport and ablation were 10-20% for iron. This result can not be compared directly with experimental results for electrothermal launchers, since the only experimental data available is integrated over the entire run time of a pulsed device. Still, it is encouraging that the calculated transmission fractions are consistent with values in the literature of between 5% and 20%.

One limitation of the current model is its inability to model flow that separates from the wall. Future upgrades should replace the forward-marching solution procedure with one that does not have this limitation. This could be done in the present code by adding an outer iteration loop, but the resulting run time would be prohibitive.

The treatment of ablation and energy transport at the wall used in the TURBFIRE code is very simple. Although the models for internal energy, average ionization state and all plasma properties have been coded in a way that will work for different bulk plasma and ablated species, the code has only been run for cases in which the ablated and bulk species are the same. This limits the cases that can be run to those on which the electrothermal launcher barrel and source sections are composed of the same material. In most electrothermal launcher experiments the source section has an ablative polycarbonate (such as lexan) wall, while the barrel section is designed of a more durable material, such as stainless steel. In order to model such experiments with TURBFIRE only the boundary conditions must be modified. It is expected that the results regarding turbulence, radiation and ablation will be similar with different bulk plasma and ablated species, but additional insight will doubtless be gained.

It is also suggested that future projects include a more thorough treatment of wall conduction, wall material phase changes, and interactions of radiation with molecules near the surface. Because these phenomena are not included in the

present model, TURBFIRE is limited in its ability to predict heat flux and ablation rates. Since the code has satisfied the goal of resolving the effects of radiation, turbulence and ablation, a more thorough treatment of the physics at the wall is a logical next step.

There are several other possible directions for future work. TURBFIRE could be combined with a code that models the source section of electrothermal launchers to yield a more comprehensive model. The code could also be adapted to model other devices in which plasma flows along a surface, by adding true compressibility, magnetic field terms, combustion of the surface material, or relaxing the constant-pressure constraint.

References

1. M.A. Bourham, J.G. Gilligan, M.L. Huebschman, D. Lianos and P.D. Alto, “Review of Components Erosion in Electric Launcher Technology”, IEEE Trans. Magnetics, Vol.31, pp.678-683, January 1995.

2. M.A. Bourham and J.G. Gilligan, "Erosion of Plasma-Facing Components Under Simulated Disruption-Like Conditions Using An Electrothermal Plasma Gun", Fusion Technology, Vol.26, pp.517-521, November 1994.

3. M.A. Bourham, O. E. Hankins, O. Auciello, J. M. Stock, B. W. Wehring, R. M. Mohanti and J.G. Gilligan, "Vapor Shielding and Erosion of Surfaces Exposed to a high Heat Load in an Electrothermal Accelerator", IEEE Trans. Plas. Sci., Vol. 17, No. 3, 1989.

4. T. P. Coffee, "A Two-Dimensional Model for the Combustion Chamber/Gun Tube of a Concept VIC Regenerative Liquid Propellant Gun", Technical Report BRL-TR-3341, 1992.

5. J. Eapen, "Theoretical and numerical Foundations for Simulation of Ablative Plasma Flow in Electrothermal-Chemical Mass Accelerators", Masters Thesis, North Carolina State University (1998)

6. U. Frisch, *Turbulence: the Legacy of A.N. Kolmogorov* , Cambridge University Press, 1995.

7. J. G. Gilligan, M. A. Bourham, O. E. Hankins and W. Eddy, ” "Magnetic Vapor Shielding Mechanism in Electromagnetic and Electrothermal Launchers", IEEE Trans. Magnetics, Vol. 29, 1993.

8. J. G. Gilligan and R. B. Mohanti, "Time-Dependent numerical Simulation of Ablation-Controlled Arcs", IEEE Trans. Plas. Sci., Vol. 18, No. 2, 1990.

9. D. H. Hahn and J. G. Gilligan, "Radiation Transport through a plasma Boundary Layer between Armature and Material Surfaces", IEEE Trans. on Magnetics, Vol. 27, No. 1, p. 251, January, 1991.

10. D. Hahn, "Energy Transport through the Boundary Layer", Ph. D. Dissertation, North Carolina State University (1989).

11. A. Hassanein, "Simulation of Plasma Disruptions-Induced Melting and Vaporization by Ion or electron Beam", J. Nuc. Mat., 122-123, p. 1453, 1984.

12. A. Hassanein and D. Ehst, "Dynamic of Plasma-Vapor Interactions During Plasma Disruptions", J. Nuc. Mat., 196-198, p. 680, 1992.

13. A. Hassanein and I. Konkashbaev, "Comprehensive Model for Disruption Erosion in a Reactor Environment", J. Nuc. Mat., 220-222, p. 244, 1995.

14. J. D. Hurley, "In-Bore Diagnostics and Modeling of an Electrothermal Plasma Launcher", Ph. D. Dissertation, North Carolina State University (1993).

15. E. Z. Ibrahim, "The Ablation Dominated Polymethylmethacrylate Arc", J. Phys. D: Appl. Phys., Vol 13, p. 2045, 1980.

16. W. P. Jones and B. E. Launder, "The Prediction of Laminarization with a Two-Equation Model of Turbulence", Intl Jnl of Heat Mass Transfer, Vol. 15, 1972.

17. P. Kovitya and J. J. Lowke, "Theoretical Predictions of Ablation-Stabilised Arcs Confined in Cylindrical Tubes", J. Phys. D: Appl. Phys., Vol. 17, p. 1197, 1984.

18. K. K. Kuo, *Principles of Combustion*, Wiley, 1986.

19. A. Loeb and Z. Kaplan, "A Theoretical Model for the Physical Processes in the Confined High Pressure Discharges of Electrothermal Launchers", IEEE Trans. on Magnetics, Vol. 25, No. 1,1989.

20. M. Mitchner and C. H. Kruger, Jr, *Partially Ionized Gases* , Wiley, 1973.

21. K. Miyamoto, *Plasma Physics for Nuclear Fusion*, MIT Press, 1989.

22. B. Mohammadi and O. Pironneau (editors), *Analysis of the K-Epsilon Turbulence Model*, Wiley, 1994.

23. K. Murali, "", Masters Thesis, North Carolina State University (1999)

24. L. Niemeyer, "Evaporation Dominated High Current Arcs in Narrow Channels", IEEE Trans. on Power Appar. and Sys., Vol. PAS-97, No. 3, 1978.

25. H. H. Ngo, "A Pseudo-Two-Dimensional, Time-Dependent model of the Heat and Current Transport Within an Electrothermal plasma Source", Masters Thesis, North Carolina State University (1998)

26. N. P. Orton and J. G. Gilligan, "Simulation of the Plasma-Surface Interaction in electric Launchers", IEEE Trans. on Magnetics, vol. 31, p. 640, January 1995.

27. Patankar and Spalding

28. V. C. Patel, W. Rodi and G. Scheuerer, "Turbulence Models for Near-Wall and Low Reynolds Number Flows: A Review", AIAA Jnl, Vol. 23, No. 9, 1984.

29. R. R. Peterson, G. A. Moses, "MIXERG - An Equation Of State and Opacity Computer Code", Comp. Phys. Comm., Vol. 28, 1983.

30. C. B. Ruchti and L. Niemeyer, "Ablation Controlled Arcs", IEEE Trans. on Plas. Sci., Vol Ps-14, No. 4, 1996.

31. H. Schlichting, *Boundary-Layer Theory*, McGraw-Hill, 1979.

32. W. G. Vincenti and C. H. Kruger, Jr, *Introduction to Physical Gas Dynamics,* Wiley, 1965.

33. J. Watrous, G. Moses and R. Peterson, “Z-PINCH: A Multifrequency Radiative Transport MHD Computer Code", Univ. of Wisconsin Fusion Technology Rept. UWFDM 584, 1984.

34. F. M. White, *Viscous Fluid Flow*, McGraw-Hill, 1991.

35. D. C. Wilcox, *Turbulence Modeling for CFD*, DCW Industries, 1993.

36. D. C. Wilcox, "Comparison of Two-Equation Turbulence Models for Boundary Layers with Pressure Gradient", AIAA Jnl., Vol. 31, No. 8, 1993..

37. C. L. Yaws, *Handbook of Thermal Conductivity, Vol. 4, Inorganic Compounds and Elements,* Gulf Publishing, 1997.

38. Y. B. Zeldovich sad Y. P. Raizer, *Physics of Shock Waves and High-Temperature Hydrodynamic Phenomena,* Vol. I, Academic Press, 1966.

39. D. Zoler, S. Cuperman, J. Ashkenazy, M. Caner and Z. Kaplan, "A Time-Dependent Model for High-Pressure Discharges in Narrow Ablative Capillaries", J. Plasma Physics, Vol. 50, Part 1, 1993.

APPENDICES

A.1 TURBFIRE Code Description

```
ccccccccccccccccccccccccccccccccccccccccccccccccccccccccccccccccccccccccccccccccccccccc
c                                                                                      c
c     TURBFIRE:  written by Nigel P. Orton                                             c
c                                                                                      c
c     TURBFIRE models turbulent and/or laminar boundary layer flows with               c
c     radiation transport, in 2-D.  Flow is modeled as incompressible but              c
c     thermally expandable (eg pressure is constant).  It uses the k-omega             c
c     turbulence model, with an option for low Reynold's number terms.  Step           c
c     sizes are variable in both the parallel (x) and perpendicular (y)                c
c     directions.                                                                      c
c                                                                                      c
c     Units: SI                                                                        c
c                                                                                      c
c     Turbulence model is based on the book:  Turbulence Modeling for CFD              c
c                                             by David C. Wilcox                       c
c                                                                                      c
c     Radiation transport model is based on the book:                                  c
c           Physics of Shock Waves and High Temperature Gas Phenomena                  c
c           by Y. B. Zeldovich and Y. P. Raizier                                       c
c                                                                                      c
c     DESCRIPTION of some VARIABLES                                                    c
c     -----------------------------                                                    c
c     ix = x-direction mesh index.  ix=2 is at the leading edge (x=0).  The            c
c          first calculations are done at ix=3.                                        c
c     iy = y-direction mesh index.  iy=1 is the wall.                                  c
c     dx and dy are the mesh spacings in the x- and y-directions.                      c
c     str is the factor by which dy increases with each iy:  y(iy)=str*y(iy-1)         c
c     nx and ny are the maximum number of gridpoints in the x- and y-                  c
c               directions.  The code stops at x=nx (if the user hasn't                c
c               stopped it earlier)                                                    c
c     niter is the maximum allowed iterations.  An error message is printed           c
c           if this is reached.                                                        c
c     ngrp is the number of radiation frequency groups                                 c
c                                                                                      c
c     phi(ieqn,i,iy) = dependent variables, where i=1 for ix-2                         c
c                                               i=2 for ix-1                         c
c                                               i=3 for ix                           c
c          phi(1,-,-) = u, flow velocity in the x-direction (m/s)                      c
c          phi(2,-,-) = U, internal energy [J/kg]  (isw(25)=1)                         c
c                     = T, temperature [K]  (isw(25)=0) Const Cp only!                 c
c          phi(3,-,-) = v, flow velocity in the y-direction (m/s)                      c
c          phi(4,-,-) = k, turbulent kinetic energy (J/kg)                             c
c          phi(5,-,-) = omega, turbulence specific dissipation rate (1/s)              c
c          phi(6,-,-) = total density (kg/m^3)                                         c
c                = density of ablated species + density of bulk plasma species       c
c          phi(7,-,-) = density of ablated species (kg/m^3)                            c
c               This is assumed to be 0 at the freestream & inlet.                     c
c               The code must be modified to run a case where that's not true!         c
c          phi(8,-,-) = radiation energy density of current freq. group.               c
c                      (phi(8,...) is used to calculate rad'n energy density,          c
c                       which is stored permanently as erad(ig,ix,iy))                 c
c     tmr(iy)= T, temperature (K or J/kg)                                              c
c     erad(ig,ix,iy) = radiation energy density of freq. grp. ig                       c
c     phifs(ieqn) = free stream B.C. for u, T, v, k, w, rho, rhoa                      c
```

```
c     phiw(ieqn)  = wall B.C. for u, T, v, k, w, rho, rhoa                    c
c     visc(iy) = fluid viscosity (kg/m/s)                                    c
c     visct(3,iy) = turbulent (eddy) viscosity (kg/m/s)                      c
c     thcond(iy) = thermal conductivity                                      c
c     radcond(iy) = radiation conductivity                                   c
c     zbar(iy) = fractional ionization (used in eqn of state)                c
c     htflux = heat flux in the y-direction                                  c
c                                                                            c
c     a(iy),b(iy),c(iy),d(iy) = matrix coefficients for pde's                c
c                                                                            c
c     isw(i) = switches:                                                     c
c         isw(1) =0 use wall fric. vel to calc y+&u+                         c
c                =1 use skin friction from Schlichting                       c
c         isw(2)=0 include zbar in eqn of state and specific heat            c
c                  calculations, but no radiation energy                     c
c               =1 include both                                              c
c               =ix (>3) run w/ zbar but no RT until ix, then add RT         c
c         isw(3)=0 for outer k & omega BC: phi=constant                      c
c               =1                         dphi/dy = 0                     c
c         isw(4)=0   for laminar flow only                                   c
c               =1   solves turbulent equations from start.                  c
c               =n   solves laminar equations up to Re=n, then adds          c
c                       k-omega calculation  (set n=critical Re)             c
c         isw(5) manages dxfrac (max allowed dx/blwidth)                     c
c         isw(6) manages dxinc (max allowed dx increment at next ix)         c
c         isw(7)=0  input constant profiles (read from 'kwgr.in')            c
c               =1  input turbfire output profiles ('profile1.in')           c
c               =2  input setebl output profiles ('profile2.in')             c
c               =3  input eddybl2  output profiles ('profile3.in')           c
c               =5  test spht model & stop execution in subroutine init      c
c         isw(8) unused                                                      c
c         isw(9) =0/1 for low/high Reynolds number terms included            c
c         isw(10)=0 calculate zbars from Saha eqn                            c
c                =1 interpolate zbars from a table.                          c
c                    (the code generates the table in subroutine INIT,       c
c                                then switches isw(10) from 1 to 2.)         c
c                =2 interpolate zbars from table.                            c
c                =-1 constant zbar=10.0e-29 (code switches to this for       c
c                                            runs at low temperatures.)      c
c         isw(11)=0/1/2/3/4/5 for screen output none/little/more/...         c
c                =-1 for outputing graph profiles to screen                  c
c                =n > 5, isw(11) is set equal to 5 when ix.ge.n              c
c         isw(12)=0 shows plots at last iteration of specified locations     c
c                =1 shows plots at every iteration of spec. locations        c
c                =2 shows plots at every iteration and location              c
c                =3 shows plots at last iteration of every location          c
c                >3 shows plots at last iteration of every isw(12)th         c
c                   location                                                 c
c         isw(13)=0 solves w conservation eq. all the way to wall            c
c                =1 solves near wall w eq. for iy < 11 & y+ < 2.5            c
c         isw(14) unused                                                     c
c         isw(15)=1 for 3 point (2nd order Taylor Series expansion)          c
c                otherwise use a central difference                          c
c         isw(16)=0 zeroth order Taylor Series expansion coefficients        c
c                                (used for guessing at next ix values)       c
c                =1 first order                                              c
c                =2 second order                                             c
c         isw(17)=0 Sutherland laminar viscosity model (low T gas)           c
c                =1 High temp. neutral & ion collision viscosity model       c
c                =-1 constant fluid viscosity (but not eddy visc!)           c
```

```
c         isw(18)=0/1  for planar/ cylindrical geometry (radius R)             c
c         isw(19)=0 write all of TURBFIRE variables into profile1.in           c
c                =1 read MAGFIRE's v,T,rho and write into profile1.in          c
c         isw(20)=1  initially specify density bc at freestream                c
c              (code will calculate P and the bc's at the wall)                c
c                =2(default)  specify pressure (it's constant!)                c
c                    (code will calculate density bc's at wall & fs)           c
c         isw(21) chooses thermal conductivity model:                          c
c                =0 MAGFIRE Low T model                                        c
c                =1 MAGFIRE high T model                                       c
c             =2 Low T model & Huu's plasma model combined (best!)            c
c             =3 Plasma model from Huu Ngo's thesis                           c
c         isw(22)=0 single species                                             c
c                >3 add ablation at ix=isw(22)                                 c
c         isw(23)=0/1 exclude/include dens*betstar*k*w in e eqn                c
c         isw(24)=0 constant specific heat                                     c
c                =1 specific heat=dU/dT                                        c
c         isw(25)=0/1 CpT (&const. Cp) / Int'l E                               c
c         isw(26) unused                                                       c
c         isw(27)=1 turns off radiation source term in E eqn (radsrc=0)        c
c                =2 same as =1 but only lasts for 1 x-step, after             c
c                                          which isw(27) is set to 0          c
c                =0 radiation source is calculated from RT eqn                c
c         isw(28)=1 offer option to print every time a plot is made            c
c                =0 print every time without prompting                         c
c                =2 print only at xout's (without prompting)                   c
c         isw(29)=1 for non-reentrant bc for Erad at the wall                  c
c                =0 for forward/reverse bc for Erad at the wall                c
c                =2 for partial current b.c.                                   c
c                                                                              c
c     con(i) = constants:                                                      c
c         con(1)= universal gas constant, R=8.3144125 [J/K-mol]                c
c         con(2)= beta                                                         c
c         con(3)= beta star                                                    c
c         con(4)= alpha                                                        c
c         con(5)= sigma k                                                      c
c         con(6)= sigma w                                                      c
c         con(7)= Boltzman's constant=1.38065812D-23                           c
c         con(8)= turbulent Prandtl # =0.89                                    c
c         con(9)= electron charge, e=1.6021773349e-19 [J/eV]                   c
c         con(10)=electron mass= 9.109389754e-31 [kg]                          c
c         con(11)=Planck's constant=6.626075540e-34 [J*s]                      c
c         con(12) unused                                                       c
c         con(13)=11604.447 [K/eV]                                             c
c         con(14)=Avagodro's # =6.022136736e+23 [1/mol]                        c
c         con(15)=pi                                                           c
c         con(16)=permittivity of free space =8.854187817d-12 [F/m]            c
c         con(17)=Bohr radius=5.29177249e-11 [m]                               c
c                                                                              c
c     file output:                                                             c
c      xout is downstream positions you want output.                           c
c      lout is desired number of outputs listed in kwsf.in file.               c
c      output is also given at the last ix position in the run                 c
c      iprof1=n is output to file 'profile1.in' at nth xout listed.            c
c     graph output:  (uses pgplot)                                             c
c      iplot is variables of ieqn to be shown                                  c
c      nxplot, nyplot are allocated columns, rows for the plots                c
c      xmax, ymax are graph maximum x and y dimensions                         c
c      plotdev is device to be used for plot (could use /XTERM or /ps)         c
c      iplot(i)=1 plots, =0 doesn't                                            c
```

```
c       i=1:  u vs y           i=2:  U vs y       i=3:  v vs y               c
c       i=4:  k vs y           i=5:  omega vs y   i=6:  density vs y         c
c       i=7:  T vs y           i=8:  zbar vs y    i=9:  Cv vs y              c
c       i=10: visc vs y        i=11: visct vs y   i=12: u+ vs y+             c
c       i=13: zbar vs T        i=14: Cv vs T      i=15: U vs T               c
c                                                                            c
c      other input variables:                                                c
c       nsp is the number of species                                         c
c       atwt and natomic are atomic weights and numbers for each species     c
c       istatemax is the number of ionization states considered when         c
c          calculating average ioni=zation states                            c
c       hsub is the heat of sublimation of the ablated species               c
c       ablfrac is the fraction of energy incident on the surface that goes  c
c          into ablation.  It can be manipulated during the run by using     c
c          ablfinc and ablfmax                                               c
c       table contains tha name(s) of the table(s) of opacities for each     c
c          species                                                           c
c       ntb and npb are the number of temperatures and pressures in the      c
c          opacity tables                                                    c
c       crit are the convergence criteria for each iteration loop            c
c       pot is the matrix of ionization potentials for each species          c
c                                                                            c
ccccccccccccccccccccccccccccccccccccccccccccccccccccccccccccccccccccccccccccc

Descriptions of Subroutines:
INIT initializes variables and begins the code run
TURB is the framework for the solution of the pde's
COEFF calculates tridagonal matrix coefficients for each pde
SOURCE calculates source terms for momentum, energy, k and omega equations
SOLVE solves the matrix equation Ax=b by forward elimination & back substitution
RADTR solves the multigroup radiation transport equations
NEXTX prepares for the next x-step
AVGZBAR calculates avg ionization state from the Saha equation & density from the
       equations of state
ABLDENS calculates density of the ablated species by solving its continuity
       equation
VISCOS solves for viscosity and thermal conductivity
EDDYVISC calculates eddy viscosities and low Reynold's # terms
GREEK calculates gamma, delta and theta coefficients for the k & omega eqns ...
INTERP determines the tabulated values of temperature and density that bracket the
       temperature and density at the point (ix,iy).
LOGINTERP interpolates a value "quan" at point
       (ix,iy), for each frequency group.  quan is interpolated from
       values tabulated at specific temperatures and densities.
INTEGRATE uses Simpson's rule to numerically integrate Erp (the equilibrium
       radiation energy density) over a frequency group.
SCREEN prints stuff out to the screen
PLOT uses the PGPLOT library to plot up to 9 graphs at once to the screen,
       then offers the option to write them to a .ps or graphics file ...
OUT prints output to files
```

A.2 Sample TURBFIRE Input File

```
$TEST
       niter=1000,
       dx=1.0D-2,  dxmax=0.0015,
       dxinc=0.15, 1.0, 1.015,
       dxfrac= 0.4, 0.4,

       ny=150,  nx=50000,  str=1.1,  dy(2)=5.D-8,
       psi=0.3,  radius=1.D-3,

       nsp=1, species= 'iron', 'iron',
       atwt= 55.8452, 55.8452,
       natomic=26, 26,
       table='iron.tbl', table2='iron.tbl'
       istatemax=7,

       hsub=6.88d-19, ablfrac=0.3333, ablfmax=1.0, ablfinc=1.00,
       Smu=110.3333, Sth=194.0, visc0=184.65D-7,
       gama=1.4, chih=0.0, a0=3.0D-10,
       viscrat=0.000001,  ntb=200,  npb=200,

       isw(1)=0,isw(2)=0,isw(3)=1, isw(4)=200000, isw(5)=120,isw(6)=230,
       isw(7)=0, isw(9)=1,  isw(10)=1, isw(11)=0, isw(12)=3,
       isw(13)=1, isw(14)=0, isw(15)=4, isw(16)=0, isw(17)=1, isw(18)=0,
       isw(19)=0, isw(20)=2, isw(21)=2, isw(22)=185, isw(23)=0, isw(24)=1,
       isw(25)=1, isw(26)=0, isw(27)=2, isw(28)=2, isw(29)=2, isw(30)=0,

       relax1= 0.25,   0.5,    0.5,
       ngrp=20,

       crit=  1.0d-6,  1.0d-5,  2.0d-4,  1.0d-9,  0.0,

       xout= 0.125, 0.1307, 0.13075, 0.1308, 0.13085,
             0.13095, 0.1405, .1425, 1.5, 2.0,
       lout=10, iprof1=0,
       iplot= 1, 1, 0, 0, 0, 0, 1, 0, 0, 0, 0, 0, 0, 0, 1, 0, 1, 0, 1, 0,
       nxplot=-2, nyplot=3,
       xmax= 5.d-3, 5.d-3, 5.d-3, 5.d-3, 5.d-3, 5.d-3, 5.d-3, 3.d-2, 1.d-2,
        3.d-2, 3.d-2, 5e-5,  0., 0., 4.0, 3., 3., 3.,   0.,
       ymax= 1.1, 4.e7, 0.1e0,  6.0e2, 2.0e6, 150., 1.1, 1.0, 1.0e4,
        1.0e-4, 4.e-4, 150., 0.0, 0.0, 100.0 , 3.0, 12.0, 0.0005, 0.,0.,

       con(1)=8.3144126,  con(2)=.075,  con(3)=0.09,
       con(4)=.556,  con(5)=0.5,  con(6)=0.5,  con(7)=1.38065812d-23,
       con(8)=0.89,  con(9)=1.6021773349d-19,  con(10)=9.109389754d-31,
       con(11)=6.626075540d-34,
       con(13)=11604.447, con(14)=6.022136736d+23,
       con(16)=8.854187817d-12, con(17)=2.800285e-21,

       tw=9710.0,  tfs=2.5,
       phifs(1)=
           2000.0,   0.0,   0.0,    0.1,  0.0,  0.0,
       phiw=
          0.0,   0.0,   0.0,    0.0,  0.0,  0.0,
       pressure=2000.0,
```

```
      pot(1,1)=0.0,
      pot(1,2)=762.5, pot(1,3)=1561.9, pot(1,4)=2957.0,
      pot(1,5)=5290.0, pot(1,6)=7240.0, pot(1,7)=9560.0,
      pot(1,8)=12060.0, pot(1,9)=14580.0, pot(1,10)=22540.0,
      pot(1,11)=25290.0, pot(1,12)=28000.0, pot(1,13)=31920.0,

      pot(2,1)=0.0,
      pot(2,2)=762.5, pot(2,3)=1561.9, pot(2,4)=2957.0,
      pot(2,5)=5290.0, pot(2,6)=7240.0, pot(2,7)=9560.0,
      pot(2,8)=12060.0, pot(2,9)=14580.0, pot(2,10)=22540.0,
      pot(2,11)=25290.0, pot(2,12)=28000.0, pot(2,13)=31920.0,
$END
```